Inorganic Chemistry

Article

Electronic Structure and Magnetic Properties of a Titanium(II) Coordination Complex

Eva M. Zolnhofer, Gayan B. Wijeratne, Timothy A. Jackson,* Skye Fortier, Frank W. Heinemann, Karsten Meyer, J. Krzystek, Andrew Ozarowski, Daniel J. Mindiola, and Joshua Telser*

Read Online

ACCESS | Metrics & More | Article Recommendations | Supporting Information

ABSTRACT: Stable coordination complexes of Ti^{II} ($3d^2$) are relatively uncommon, but are of interest as synthons for low oxidation state titanium complexes for application as potential catalysts and reagents for organic synthesis. Specifically, high-spin Ti^{II} ions supported by redox-inactive ligands are still quite rare due to the reducing power of this soft ion. Among such Ti^{II} complexes is *trans*-[TiCl$_2$(tmeda)$_2$], where tmeda = N,N,N',N'-tetramethylethane-1,2-diamine. This complex was first reported by Gambarotta and co-workers almost 30 years ago, but it was not spectroscopically characterized and theoretical investigation by quantum chemical theory (QCT) was not feasible at that time. As part of our interest in low oxidation state early transition metal complexes, we have revisited this complex and report a modified synthesis and a low temperature (100 K) crystal structure that differs slightly from that originally reported at ambient temperature. We have used magnetometry, high-frequency and -field EPR (HFEPR), and variable-temperature variable-field magnetic circular dichroism (VTVH-MCD) spectroscopies to characterize *trans*-[TiCl$_2$(tmeda)$_2$]. These techniques yield the following $S = 1$ spin Hamiltonian parameters for the complex: $D = -5.23(1)$ cm^{-1}, $E = -0.88(1)$ cm^{-1}, ($E/D = 0.17$), $\mathbf{g} = [1.86(1), 1.94(2), 1.77(1)]$. This information, in combination with electronic transitions from MCD, was used as input for both classical ligand-field theory (LFT) and detailed QCT studies, the latter including both density functional theory (DFT) and *ab initio* methods. These computational methods are seldom applied to paramagnetic early transition metal complexes, particularly those with $S > 1/2$. Our studies provide a complete picture of the electronic structure of this complex that can be put into context with the few other high-spin and mononuclear Ti^{II} species characterized to date.
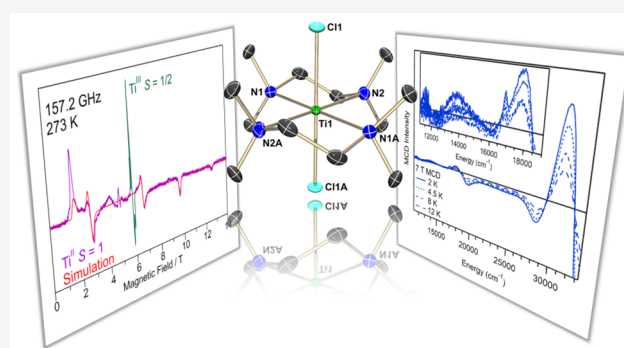
INTRODUCTION

Titanium(II), $3d^2$, is a relatively uncommon oxidation state for this group 4 metal, even in organometallic complexes. For example, in contrast to the commonly found neutral 3d metallocenes, MCp_2 ($Cp = \eta^5\text{-}C_5H_5^-$; M = V, Cr, Mn, Fe, Co, Ni), there is no thermally stable $TiCp_2$.[1,2] Extensive substitution of the cyclopentadienyl framework is necessary to stabilize a mononuclear metallocene.[3] Considering traditional coordination complexes, halide-bridged complexes result with many commonly used ligands, such as THF.[4,5] Aqueous Ti^{II} has been reported relatively recently,[6] and there are stable, mononuclear coordination complexes such as with pyridine (py), *trans*-[TiCl$_2$(py)$_4$],[7] the electronic structure of which was the subject of a previous study by some of us.[8] This system showed a very intriguing electronic structure, characterized by a nearly orbitally degenerate ground state and large zero-field splitting (zfs; modeled using an $S = 1$ spin Hamiltonian as $D \approx 60$ cm^{-1}). A related type of ligand that affords stable, mononuclear coordination complexes of Ti^{II} is $R_2ECH_2CH_2ER_2$, where E = N, P; R = typically CH_3 (Me).

For E = N, the ligand is N,N,N',N'-tetramethylethane-1,2-diamine (tmeda), and for E = P, the ligand is 1,2-bis(dimethylphosphino)ethane (dmpe). The complexes are of general formula *trans*-[TiX$_2$(Me$_2$ECH$_2$CH$_2$EMe$_2$)$_2$], where $X^- = Cl^-$,[9] CH_3^-,[10] $\eta^2\text{-}BH_4^-$,[11] OPh^-,[12] for E = P, but only the chloride for E = N.[13] The *trans*-[TiX$_2$(dmpe)$_2$] series is of interest since, as noted by Girolami and co-workers,[10−12] it can be divided into two classes by spin ground state: for X = OPh and Me, the complexes are diamagnetic, while for the others (halides and tetrahydroborate), the ground state is a spin triplet, which is also the case for both *trans*-[TiCl$_2$(py)$_4$] and *trans*-[TiCl$_2$(tmeda)$_2$]. Herein, we focus on the sole N-donor complex, *trans*-[TiCl$_2$(tmeda)$_2$], wherein the tmeda ligand is
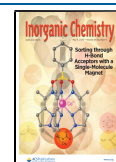
less redox active than dmpe, thus rendering the Ti^{II} oxidation state less ambiguous, yet the complex itself is redox active.[14] We provide a detailed spectroscopic and computational investigation using experimental and computational techniques that were unavailable to either the Girolami[10−12] or Gambarotta[13−16] groups roughly 30 years ago. In contrast to the dmpe series, with tmeda only σ-interactions are possible and the lighter atom N and Cl donors are less computationally challenging than the combination of P and Br/I. The high symmetry of the complex is also helpful for computational analysis, particularly for classical ligand-field theory (LFT). Moreover, the present investigation on the electronic structure of trans-[TiCl$_2$(tmeda)$_2$], including its comparison with the closely related, yet distinctly different complex, trans-[TiCl$_2$(py)$_4$],[8] can also shed light on the interesting reactivity of mononuclear Ti^{II} complexes, such as the reductive coupling of acetonitrile.[16]

■ EXPERIMENTAL SECTION

General Synthesis Considerations. Manipulation of air-sensitive compounds was performed using standard Schlenk-line techniques or an MBraun inert-gas glovebox containing an atmosphere of purified dinitrogen or argon where specified. Solvents were purified using a two-column solid-state purification system (Glasscontour System, Joerg Meyer, Irvine, CA), transferred to the glovebox without exposure to air and stored over activated molecular sieves and/or sodium metal. NMR solvents were dried over Na/K alloy or molecular sieves and distilled under reduced pressure and/or filtered through a column of neutral activated aluminum oxide. Elemental analysis results were obtained from the Analytical Laboratories at the FAU Erlangen-Nürnberg, using Euro EA 3000 (Euro Vector) and EA 1108 (Carlo-Elba) elemental analyzers.

Synthesis of trans-[TiCl$_2$(tmeda)$_2$]. The procedure of Edema et al.[13] was used with slight modifications. Under an argon atmosphere, TiCl$_3$(THF)$_3$ (6.85 g, 0.018 mmol, 1 equiv)[17] was dissolved in THF (80 mL). After addition of Li granules (0.43 g, 0.069 mmol, 3.8 equiv) and tmeda (13.05 g, 16.84 mL, 0.112 mmol, 6.2 equiv), a color change to dark green was observed. After the reaction was stirred overnight, the resulting brown suspension was decanted in order to remove the residual Li, and it was diluted with THF (45 mL). Under a nitrogen atmosphere, the suspension was filtered over Celite. The dark brown filtrate was concentrated to a volume of 70 mL and filtered, giving a light violet filter cake, which was washed with cold (−35 °C) THF (2 × 0.5 mL) and dried to give the product as a light purple powder. A second crop was collected by further concentrating the dark brown filtrate to a volume of 30 mL, followed by filtration, washing, and drying, as with the first crop. Both crops were combined to give the product as a light violet powder (1.59 g, 0.005 mmol, 25%)

Anal. (%) Calcd for C$_{12}$H$_{32}$Cl$_2$N$_4$Ti (MW = 351.18 g/mol): C, 41.04; H, 9.18; N, 15.95. Found: C, 40.98; H, 9.29; N, 15.92.

X-ray Crystallography. Details of the X-ray crystallography of trans-[TiCl$_2$(tmeda)$_2$], collected at 100 K, are given in Supporting Information, section S1, which includes Figure S2 that shows the crystal packing diagram for the complex, demonstrating that there are no intermolecular interactions.

Magnetometry. Magnetization data of crystalline, finely powdered trans-[TiCl$_2$(tmeda)$_2$] restrained within a polycarbonate gel capsule were recorded with a Quantum Design MPMS-XL SQUID magnetometer (FAU Erlangen-Nürnberg). DC susceptibility data for two separate samples (45.6 mg and 36.2 mg, respectively) were collected in the temperature range of 2−300 K under a DC field of 1 T. Temperature dependent magnetization data were recorded for one sample at four external magnetic fields (in T): 0.1, 1.0, 3.0, 5.0. Values of the magnetic susceptibility were corrected for core diamagnetism of the sample estimated using tabulated Pascal's constants.[18] The programs DSUSFITP (J. Telser) was used for fitting magnetic susceptibility data and JulX (E. Bill, MPI-CEC, Mülheim, Germany)

for fitting magnetization data, both using a standard S = 1 spin Hamiltonian.

Magnetic Circular Dichroism Spectroscopy. Magnetic circular dichroism (MCD) spectra of a mull sample of trans-[TiCl$_2$(tmeda)$_2$] were collected using a spectropolarimeter (Jasco J-815) interfaced with a magneto-optical cryostat (Oxford Instruments SM 4000−8). The mull sample was prepared by mixing solid complex with a minimum amount of Fluorolube and grinding the sample using a mortar and pestle until a homogeneous mull was obtained. The mull was then spread between two quartz discs and inserted into a custom-made sample holder. All sample manipulations were performed in an argon-filled glovebox. The sample was immediately flash frozen upon removal from the glovebox and stored under liquid nitrogen prior to data collection. During data collection, the sample was kept at low temperature under a helium atmosphere. MCD data presented here represent the difference of spectra collected at positive and negative fields of the same magnitude. Deconvolution of MCD data were performed using Igor 6.32A (Wavemetrics). The fitting of variable-temperature, variable-field (VTVH) MCD data was performed using a program developed by Neese and Solomon.[19]

High-Frequency and -Field EPR Spectroscopy (HFEPR). HFEPR data were acquired using either of two facilities located at the NHMFL. The EMR Facility includes a spectrometer described elsewhere,[20] modified by the use of Virginia Diodes Inc. (VDI, Charlottesville, VA) sources, operating in a 50−420 GHz frequency range. The spectrometer is associated with a 15/17-T super-conducting magnet. The DC Facility includes a setup using tunable sources (backward wave oscillators, BWOs), routinely operating in a 100−700 GHz frequency range and associated with the 25-T resistive Bitter-type "Keck" magnet. In both cases an InSb bolometer (QMC, Cardiff, Wales, U.K.) is used as a detector. The necessary modulation was obtained either through modulating the magnetic field ("magnetic modulation") or chopping the sub-THz wave beam ("optical modulation"). In both cases the signal was converted from AC to DC by a lock-in amplifier (Stanford SR-830). The samples were handled under inert atmosphere. Approximately 40 mg of micro-crystalline trans-[TiCl$_2$(tmeda)$_2$] was employed in each case. Simulations of HFEPR spectra used the program SPIN written by A. Ozarowski.

Computational Methods. All quantum chemical electronic structure calculations were performed using ORCA 3.0.[21,22] These results were compared with those obtained using the newer ORCA 4.1.2 release using one trans-[TiCl$_2$(tmeda)$_2$] structure. The electronic transition energies and zfs parameters were very similar between these two versions (Table S2). In particular, the zfs parameters were within 0.06 cm^{-1} and the electronic transition energies were within 1000 cm^{-1} (and typically within 200 cm^{-1}). The ORCA 4.1.2 version also permits the calculation of D_{SSC} using the CASSCF method. This calculation yielded D_{SSC} = −0.35 cm^{-1}, which is similar in magnitude, but opposite in sign, to that obtained from a SORCI calculation (D_{SSC} = +0.51 cm^{-1}). Both constrained and full geometry optimizations of trans-[TiCl$_2$(tmeda)$_2$] were performed. Constrained optimizations started with the coordinates from the present structure or those published by Edema et al. (CSD code: KIKKUZ),[13] and the positions of the hydrogen atoms were optimized using the BP functional[23,24] and TZVP (Ti, N, and Cl) and SVP (C and H) basis sets.[25,26] Full geometry optimizations, which included energy minimization with respect to all nuclear coordinates, were performed using the BP,[23,24] B3LYP,[27−29] B3LYP-D3,[30,31] M06-L,[32−34] TPSSh,[35] and TPSSh-D3[30,31] functionals. In each of these cases, TZVP (Ti, N, and Cl) and SVP (C and H) basis sets were employed.[25,26] To assess the impact of basis set size on the optimized structure, separate optimizations with the BP functional were carried out using the def2-TZVP (Ti, N, and C) and def2-SVP (C and H) basis sets,[36,37] and the TZVPP (all atoms) basis set.[36] All calculations using pure functionals employed the resolution of the identity (RI) approximation,[38] while calculations featuring hybrid functionals utilized the RIJCOSX[39] approximation. In all cases where the RI or RIJCOSX approximations were used, the appropriate auxiliary basis sets (i.e., SV/J or TZVP/J) were employed. A truncated model of

trans-[TiCl$_2$(tmeda)$_2$], in which the *N*-methyl moieties were replaced by hydrogen atoms (referred to as *trans*-[TiCl$_2$(eda)$_2$]), was also generated from the X-ray diffraction (XRD) coordinates in this work. This modified model was then subjected to a constrained optimization, where only the positions of the H atoms were energy minimized. This calculation used the BP functional[23,24] and TZVP (Ti, N, and Cl) and SVP (C and H) basis sets.[25,26] Cartesian coordinates for all complexes are included in the Supporting Information (Tables S3–S13).

Ground-state spin Hamiltonian parameters and electronic transition energies were calculated using DFT, CASSCF (with and without NEVPT2 corrections), and SORCI methods. State-averaged CASSCF calculations using second-order-N-electron valence state perturbation theory (NEVPT2)[40] were used for structures of *trans*-[TiCl$_2$(eda)$_2$] based on the crystal structure reported in this work, that previously reported by Edema et al.,[13] and a truncated model. These calculations utilized TZVP (Ti, N, and Cl) and SVP (C and H) basis sets.[25,26] Because the RI approximation was employed, the SV/C and TZV/C auxiliary basis sets were also used. Quasi-restricted orbitals, obtained from a single-point DFT computation, provided an initial guess for the CASSCF wave function. An active space consisting of all Ti^{II} 3d orbitals and electrons, CAS(2,5), was selected, and 10 triplet roots and 15 singlet roots were calculated. For certain systems, a larger active space, CAS(2,7), was employed. For the truncated *trans*-[TiCl$_2$(eda)$_2$] systems, SORCI calculations[41] were also performed. These calculations utilized the same basis sets, active spaces, initial guess orbitals, and number of triplet and singlet roots as used in the CASSCF/NEVPT2 calculations. CI thresholds were set at $T_{sel} = 10^{-6}$ hartrees, $T_{pre} = 10^{-4}$ hartrees, and $T_{nat} = 10^{-5}$ hartrees. For both the CASSCF/NEVPT2 and SORCI calculations, the "rotate" command in *ORCA* was used, when necessary, to ensure that the active space consisted of the five Ti^{II} 3d orbitals. Ground- and excited-state properties were last calculated using the perturbed (CP)[42] and time-dependent (TD)[43–46] DFT methods, respectively. The TD-DFT calculations employed the B3LYP functional,[27–29] and the RIJCOSX approximation.[39] For the CP-DFT calculations, we assessed the effect of the functional choice on the calculated zero-field splitting parameters and *g*-values. Thus, separate calculations were performed using the B3LYP,[27–29] BP,[23,24] TPSS,[35] TPSSh,[35] M06-L,[32–34] and M06[32–34] functionals. The CP-DFT and TD-DFT calculations both used TZVP (Ti, N, and Cl) and SVP (C and H) basis sets, along with the SV/J and TZVP/J auxiliary basis sets.[25,26]

RESULTS AND ANALYSIS

Crystal Structures. Edema and co-workers previously determined the molecular structure of *trans*-[TiCl$_2$(tmeda)$_2$] by an XRD structural analysis at room temperature.[13] We have modified the synthesis, obtained single crystals, and re-collected the XRD data at a lower temperature (100 K) in order to obtain more precise metrical parameters for the purpose of computational studies. Purple, block-shaped single crystals suitable for X-ray diffraction studies were obtained by cooling a concentrated solution of *trans*-[TiCl$_2$(tmeda)$_2$] in THF to −35 °C (details on crystallography are given in section S1, Supporting Information, including a table of parameters, Table S1). The molecular structure features a Ti^{II} metal center in an octahedral coordination geometry, equatorially coordinated by two bidentate molecules of tmeda and axially coordinated by two chlorido ligands, as shown in Figure 1. The crystallographic disorder in the tmeda C atoms is not shown, but is displayed in Figure S1 (Supporting Information). The crystal packing is shown in Figure S2. In agreement with Edema's molecular structure,[13] an inversion center is situated on the central Ti^{II} ion, and the carbon atoms of the tmeda ligands are found to be conformationally disordered. Due to the lower temperature, the refinement yielded a better fit (least-squares *R*-factor = 0.0280 here versus 0.072 originally[13]),
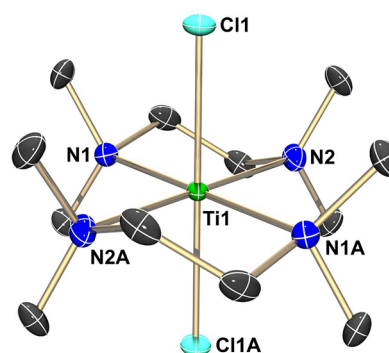
Figure 1. Solid-state molecular structure of *trans*-[TiCl$_2$(tmeda)$_2$] as determined here at 100 K in space group P2$_1$/n (no. 14). Thermal ellipsoids are shown at 50% probability. H atoms and disorder are omitted for clarity; C, gray; N, blue; Cl, cyan; Ti, green. The Ti atom is situated on a crystallographic inversion center (at coordinates 1, 0, 0.5), which results in C_i molecular symmetry (atom labels denoted with an additional A refer to the symmetry related position: −x + 2, −y, −z + 1).

and the data were collected at a better resolution (max. 2θ = 59.2° versus 44.8°). Discussion of the metrical parameters of *trans*-[TiCl$_2$(tmeda)$_2$] will be addressed in the spectroscopic and theoretical section (Table 2, *vide infra*).

Magnetic Circular Dichroism Data. Magnetic circular dichroism (MCD) spectra were collected for a mull sample of *trans*-[TiCl$_2$(tmeda)$_2$] at a range of temperatures (2−12 K) and magnetic field strengths (1−7 T).[47] In the spectral window of 11 000−33 300 cm^{-1}, at least eight temperature-dependent features are observed (Figure 2); additional MCD
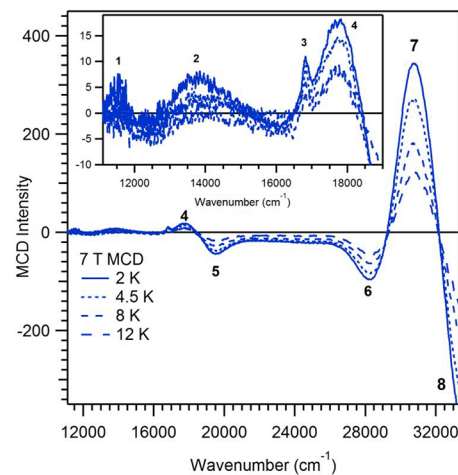
Figure 2. Variable-temperature, 7 T MCD spectra of a mull sample of *trans*-[TiCl$_2$(tmeda)$_2$]. The inset shows an expanded view of the weak bands (1 through 4) found in the lower-energy region.

spectra, showing a Gaussian deconvolution of the electronic transitions, are provided in Figure S3. Temperature-dependent MCD signals (*C*-terms) arise from electronic transitions originating from paramagnetic ground states,[19,48,49] such as the spin triplet ground-state expected for *trans*-[TiCl$_2$(tmeda)$_2$]. *C*-terms with a derivative-shape, where adjacent positive and negative MCD features have roughly equal intensity, are referred to as pseudo-*A* terms. These terms arise from excitations to orbitally degenerate excited states, or nondegenerate excited states of similar energy that interact by

spin−orbit coupling.[19,48,49] In the MCD spectrum of *trans*-[TiCl$_2$(tmeda)$_2$], bands 4 and 5, and bands 7 and 8, give rise to two pseudo-*A* terms (Figure 2). Along with band 6, the pseudo-*A* term of bands 7 and 8 dominates the higher-energy region of the MCD spectrum and contributes most of the observed MCD intensity. In contrast, the lower-energy region (below 17 000 cm^{-1}) is composed of very weak MCD features (bands 1 through 3; see Figure 2, inset). In this region, we have labeled only MCD features whose intensities show an unambiguous increase with decreasing temperature. It is quite possible that there are negatively signed MCD features near 12 500 and 16 000 cm^{-1}, as the MCD signal drops below zero and shows variations with temperature at these energies. However, this behavior could be due to minor baseline shifts, and, thus, there is no definitive evidence for electronic transitions at these energies.

A Gaussian deconvolution of the 2 K, 7 T MCD spectrum of *trans*-[TiCl$_2$(tmeda)$_2$] provides energies and bandwidths for the eight temperature-dependent MCD features (Table 1 and

Table 1. Electronic Transition Energies (cm^{-1}), Bandwidths, $\bar{\nu}_{1/2}$ (cm^{-1}), Transition Polarizations, and Transition Assignments from Analyses of MCD Spectra and VTVH MCD Data of *trans*-[TiCl$_2$(tmeda)$_2$]

| band	energy	$\bar{\nu}$	polarization[a]			assignment (in D_{2h})
			% x	% y	% z	
1	11 560	835				^3A_g
2	13 810	835				$^3B_{3g}$
3	16 825	170				^1A_g
4	18 750	2 000				$^3B_{3g}$
5	19 050	2 000	1	4	95	$^3B_{2g}$
6	28 550	2 200	7	17	79	CT
7	30 850	2 300	1	2	97	CT
8	33 650[b]	2 400				CT

[a]Transition polarizations determined from analysis of VTVH MCD data collected for bands 5, 6, and 7. The other MCD features were too weak in intensity to yield high-quality VTVH MCD data. [b]The band maximum is not observable but estimated from a Gaussian deconvolution modeling the onset of intensity for this transition.

Figure S2). Transition polarizations for three of the more prominent MCD bands (bands 5−7) were obtained by fitting the variable-temperature variable-field (VTVH) MCD curves collected near the band maxima (Figure 3). VTVH MCD curves are sensitive to both the transition dipole moment products (M_{xy}, M_{xz}, and M_{yz}) of the electronic transition under interrogation, as well as the spin multiplicity and the spin Hamiltonian parameters of the paramagnetic ground state (i.e., g-values, axial zero-field splitting parameter, *D*, and rhombicity, *E/D*).[19,49] Thus, differences in transition polarization give rise to the modest changes in the VTVH MCD saturation behavior of bands 5, 6, and 7 (Figure 3). The transition polarization for each band was determined by floating the transition dipole moment products to best fit the experimental data, with the spin Hamiltonian parameters fixed to the values obtained from low temperature HFEPR experiments (*D* = −5.28 cm^{-1}, *E/D* = 0.17, **g** = [1.86, 1.94, 1.77]; *vide infra*). For each band, a high-quality fit was obtained with a transition moment of predominant z-polarization (Figure 3 and Table 1).

Combining the analysis of the MCD and VTVH MCD data with ligand-field theory considerations leads to tentative assignments for the MCD features. Figure 4 shows a ligand-
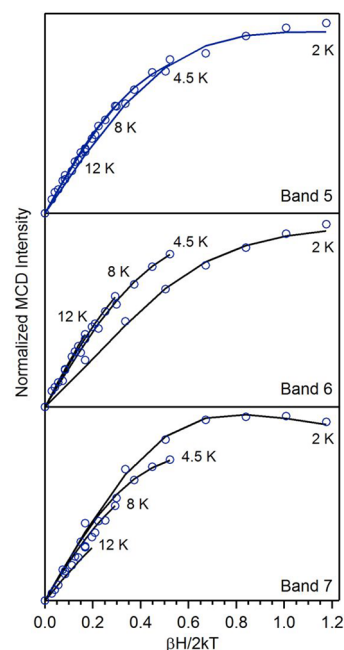
Figure 3. Experimental VTVH MCD curves for a mull sample of *trans*-[TiCl$_2$(tmeda)$_2$] (open circles) collected at 19 500 cm^{-1} (band 5, top), 28 250 cm^{-1} (band 6, center), and 30 700 cm^{-1} (band 7, bottom). Theoretical fits to these curves are overlaid on the respective plots (solid lines). These fits used the following: *S* = 1, *D* = −5.28 cm^{-1}, *E/D* = 0.16, **g** = [1.891, 1.963, 1.786], and transition polarizations in Table 1.
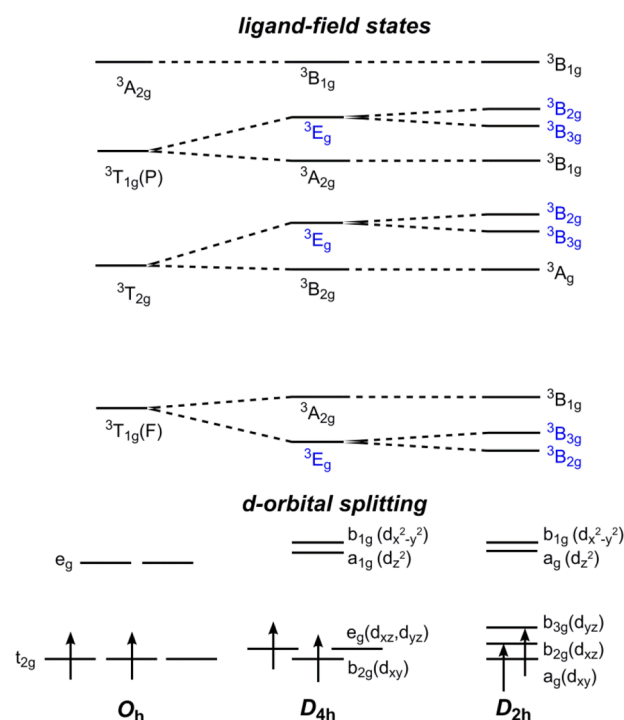
Figure 4. Ligand-field correlation diagram from O_h to D_{2h} symmetry showing only triplet states. D_{2h} states derived from parent E$_g$ states of D_{4h} symmetry are in blue. Spin−orbit mixing between these closely spaced states could give rise to MCD pseudo-*A* terms.

field correlation diagram from O_h to D_{2h} symmetry. Although the *trans*-[TiCl$_2$(tmeda)$_2$] complex is of lower symmetry, the Ti^{II} center and its first coordination sphere have D_{2h} symmetry

and only show a small deviation from D_{4h} symmetry. The crystallographic Ti−N distances (d(Ti−N) = 2.376(2) and 2.382(2) Å) are only slightly different from one another, and the bidentate tmeda ligands cause the equatorial N−Ti−N angles ($\angle$(N−Ti−N) = 79.13(4) and 100.87(4)°) to deviate from the idealized D_{4h} values by only ∼10°. Consequently, the doubly degenerate E states of the D_{4h} point group will be split into nondegenerate B_{2g} and B_{3g} states, but the splitting between these states is expected to be quite small (Figure 4). Thus, the ground-state of trans-[TiCl$_2$(tmeda)$_2$] will be orbitally nondegenerate, but with low-lying excited states. High-level multireference *ab initio* computations, described later, yield a $^3B_{2g}$ ground state, as indicated in Figure 4.

Electronic transitions to the low-lying excited states of trans-[TiCl$_2$(tmeda)$_2$] also derived from the ground $^3T_{1g}$(F) state of the parent O_h group, namely the lowest energy $^3B_{3g}$ and $^3B_{1g}$ states (Figure 4), will lie below the available energy range of our MCD experiments. Thus, the lowest-energy MCD features at 11 560 and 13 810 cm^{-1} (bands 1 and 2) most likely arise from two of the three states, ^3A_g, $^3B_{3g}$, and $^3B_{2g}$, which derive from $^3T_{2g}$ in O_h. In support, previous electronic absorption and luminescence studies of Ti^{II} doped into MgCl$_2$ and MgBr$_2$ placed the $^3T_{2g}$ excited states of these Ti^{II} centers at 9260 and 8220 cm^{-1}, respectively.[50] The shift of this state to high-energy for trans-[TiCl$_2$(tmeda)$_2$] would be consistent with the stronger ligand-field of the coordination complex. The pseudo-A term composed of bands 4 and 5 (18 750 and 19 050 cm^{-1}) is assigned to excitations to the $^3B_{3g}$ and $^3B_{2g}$ components of the $^3T_{1g}$(P) parent state. For Ti^{II}:MgCl$_2$ and Ti^{II}:MgBr$_2$, the $^3T_{1g}$(P) state was observed at 16 130 and 15 040 cm^{-1} respectively.[50] We cannot definitively identify the third component of the $^3T_{1g}$(P) parent state, namely $^3B_{1g}$. The fits suggest the possibility of signal in the range 15 000−16 000 cm^{-1} that might be due to an excitation to this state, and this is discussed in section S2 (Supporting Information). Band 6 could be assigned as an excitation to the highest-energy $^3B_{1g}$ state, which derives from the $^3A_{2g}$ parent state (Figure 4). Although this seems too high an energy for this transition (the corresponding state was observed at 19 340 cm^{-1} for Ti^{II}:MgCl$_2$), the LFT calculations described below lend some support to this possibility. In addition, the $^3B_{1g}$ state arises from a two-electron excitation, and, therefore, might be of modest intensity. Accordingly, band 6, along with bands 7 and 8, is tentatively assigned as a charge-transfer transition, which presumably involves the chlorido ligands. Unfortunately, Jacobsen et al. show absorption data only up to 25 000 cm^{-1};[50] this is too low for direct comparison with bands 6−8 seen here. Finally, band 3 (16 825 cm^{-1}), which has a much narrower bandwidth than the other MCD features (Table 1), is attributed to the intraconfigurational spin-forbidden transition to an ^1A_g excited state; this assignment is discussed in the LFT section below. Intraconfigurational transitions have only minor geometric distortions in the electronic excited state, which leads to small bandwidths.[51,52] The corresponding transition was observed at 15 935 cm^{-1} for Ti^{II}:MgCl$_2$,[50] supporting our assignment.

Magnetometry. For comparison with the more informative, but more exotic, VTVH MCD and HFEPR investigations, routine DC magnetic susceptibility measurements were performed on powder samples of trans-[TiCl$_2$(tmeda)$_2$]. The data confirmed the complex's $S = 1$ ground state and their fitting gave estimates as to the spin Hamiltonian parameters, which were in reasonable agreement with those from HFEPR

(*vide infra*). These results are shown in Figure S4, which also gives the fit parameters. The susceptibility fits demonstrate that, as is often the case,[53] it was impossible to determine the sign of the D value. Variable temperature magnetization data recorded at four fields showed the expected nested behavior (Figure S5) and were best fitted using $S = 1$ with $D = +4.98$ cm^{-1} and $g_{iso} = 1.761$. Given that adequate fits were obtained using an axial zfs and isotropic g value, no attempts were made to introduce rhombic zfs or g anisotropy in the magnetometry analysis.

High-Frequency and -Field EPR Data. High-frequency and -field EPR (HFEPR) spectroscopy was performed on powder samples of trans-[TiCl$_2$(tmeda)$_2$]. The complex gave a strong response in the frequency range of 50−700 GHz, and field range up to 25 T, from low (liquid helium, 4.2 K) to high temperature (273 K). The 4.2 K spectra were plagued by the "quasi-noise" phenomenon, i.e., incomplete averaging of the single-crystal spectra over space due to insufficient grinding.[54,55] Extensive grinding was avoided because of the sample's lability as well as air and moisture sensitivity. Much better spectra were collected at somewhat elevated temperatures due to thermally activated line broadening. An example of such a spectrum is shown in Figure 5. One can recognize a
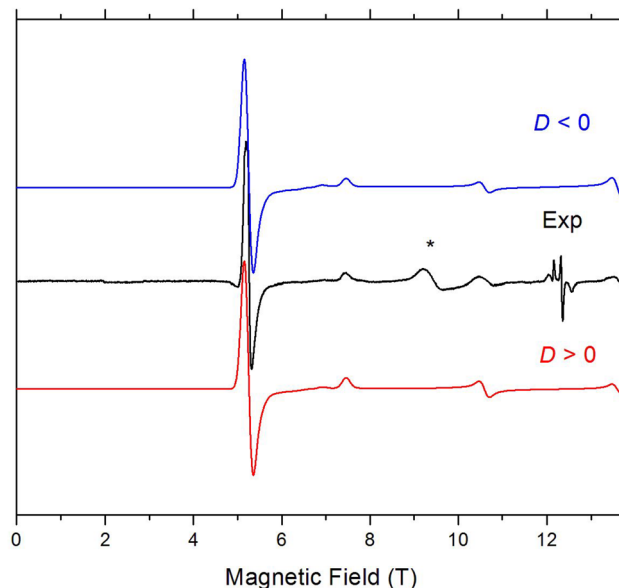

Figure 5. HFEPR spectrum of trans-[TiCl$_2$(tmeda)$_2$] recorded at 331 GHz and 30 K using magnetic modulation, resulting in a derivative shape (black trace). The colored lines are simulations using spin Hamiltonian parameters: $S = 1$, $|D| = 5.19$ cm^{-1}, $|E| = 0.89$ cm^{-1}, and $g = [1.88, 1.95, 1.80]$. Black trace: experiment. Colored lines: simulations. Blue trace: negative D; red trace: positive D. The unknown impurity resonance at ∼9.3 T marked by an asterisk is not simulated. The group of narrow signals at ∼12.5 T ($g = 1.9$) originates from a minor Ti^{III} impurity and is not simulated either.

classical triplet powder pattern, dominated by the so-called half-field transition (an off-axis turning point of the nominally forbidden $\Delta m_S = \pm 2$ transition) at 5.26 T accompanied by turning points of the allowed $\Delta m_S = \pm 1$ transitions at higher fields. Additional low-temperature HFEPR spectra collected at frequencies lower and higher from that in Figure 5 are shown respectively in Figures S6 and S7 (Supporting Information). The temperature at which the experiment shown in Figure 5

was performed (30 K) was too high and the frequency too low (331 GHz) to determine the sign of D. For that purpose, we simulated some of the best-shaped spectra collected at liquid-helium temperature, such as the one shown in Figure S7. From those simulations, the negative sign of D was firmly established through the similarity of the experimental spectra and their simulations.

The spin Hamiltonian parameters used in the spectral simulations of single-frequency spectra such as those shown in Figures S6, 5, and S7 were chosen to optimally reproduce the experiment; however, they are not completely frequency-independent. To obtain frequency-independent parameters, we followed the tunable-frequency EPR procedure,[56] and collected spectra at multiple frequencies, plotting the field vs frequency (or energy) dependence of the turning points, at 4.2 or 30 K. The resulting 2-D map is shown in Figure 6. A least-
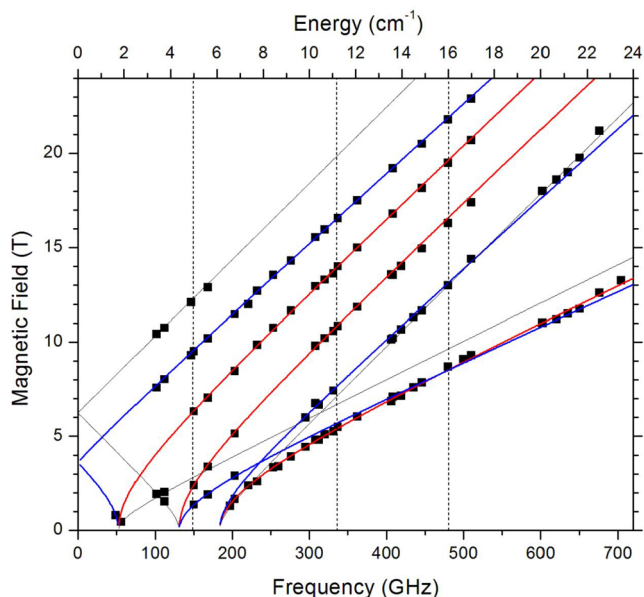
Figure 6. Field vs frequency (or energy) dependence of turning points in powder spectra of *trans*-[TiCl$_2$(tmeda)$_2$] at 4.2−30 K. Squares are experimental points; curves were simulated using best-fitted spin Hamiltonian parameters: $S = 1$, $|D| = 5.23$ cm^{-1}, $|E| = 0.88$ cm^{-1}, and **g** = [1.86, 1.94, 1.77]. Red curves: turning points with B_0 parallel to the x axis of the zfs tensor. Blue curves: $B_0 \parallel y$. Black curves: $B_0 \parallel z$. The vertical dashed lines represent frequencies at which spectra shown in Figures S6, 5, and S7 in increasing order, respectively, were recorded.

squares fit to the experimental dependencies provided the following spin Hamiltonian parameters: $S = 1$, $D = -5.23(1)$ cm^{-1}, $E = -0.88(1)$ cm^{-1}, **g** = [1.86(1), 1.94(2), 1.77(1)].

As mentioned above, *trans*-[TiCl$_2$(tmeda)$_2$] produced an EPR response at high temperature (273 K) that was surprisingly strong for a non-Kramers spin system. A typical spectrum recorded under these conditions, in this case at 157 GHz, is shown in Figure 7. Simulations were done for negative D only, since at 273 K the simulated spectra are the same for either sign of D due to the roughly equal Boltzmann populations of the ground and excited m_S levels. Analogous spectra collected at higher frequencies are shown in the Supporting Information: Figures S8 (221 GHz) and S9 (326 GHz). The $S = 1$ spin Hamiltonian parameters appear
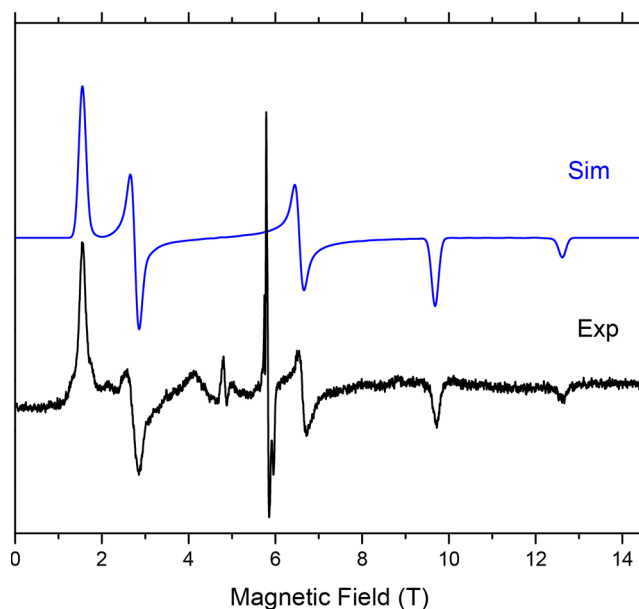
Figure 7. HFEPR spectrum of *trans*-[TiCl$_2$(tmeda)$_2$] at 157.2 GHz and 273 K using magnetic modulation, resulting in a derivative shape (black trace). The blue trace is a simulation using spin Hamiltonian parameters: $S = 1$, $|D| = 5.28$ cm^{-1}, $|E| = 0.84$ cm^{-1}, and **g** = [1.89, 1.98, 1.78]. The group of narrow signals at ~6 T ($g = 1.9$) originates from a minor Ti^{III} ($S = 1/2$) impurity and is not simulated. The weak signal at ~5 T is of unknown origin and is also not simulated.

not to change significantly from 30 to 273 K, as indicated by single-frequency simulations. To determine their values at 273 K more accurately, we again used the tunable-frequency methodology (Figure S10, Supporting Information) and obtained the following: $|D| = 5.28(1)$ cm^{-1}, $|E| = 0.857(5)$ cm^{-1}, and **g** = [1.891(2), 1.963(3), 1.786(3)].

Ligand Field Theory—Electronic Transitions and ZFS Parameters. The application of advanced computational methods using quantum chemical theory (QCT), both density functional theory (DFT) and *ab initio* methods, to the electronic structure of *trans*-[TiCl$_2$(tmeda)$_2$] is described in the next section. However, classical ligand field theory (LFT) is still instructive in this effort, as was done earlier by Güdel and co-workers on Ti^{II} dopants in halide salts[50,57] and in our previous study on *trans*-[TiCl$_2$(py)$_4$].[8] The Ti:MX$_n$ (M = Na, Mg; X = Cl, Br; n = 1, 2) species lent themselves to analysis by a crystal-field model. This model can still be applied to the covalent complex, *trans*-[TiCl$_2$(tmeda)$_2$], but we also use the angular overlap model (AOM).[58] As a first step using a crystal-field model, we ignore the tetragonal distortion present and treat the complex as octahedral, so that the only variables are the octahedral (cubic) crystal-field splitting, Dq, and the Racah parameter B, and only spin-allowed (triplet−triplet) transitions are considered (i.e., band 3 in Table 1 is ignored). This model requires averaging the three components in D_{2h} to give the parent $^3T_{1,2g}$ energies. This would be trivial if all three were observed, but this is not the case. For the energy of $^3T_{2g}$, we take here the weighted average of bands 1 and 2 (i.e., 13 060 cm^{-1}), realizing that there should be two separate components to band 2 ($^3B_{2g}$ and $^3B_{3g}$ from ^3E_g in D_{4h}), but the rhombic splitting of this band is likely small. For the energy of $^3T_{1g}$(P), a complementary difficulty obtains. The two components of ^3E_g in D_{4h} are observed (bands 4 and 5), but not $^3A_{2g}$ in D_{4h} ($^3B_{1g}$ in D_{2h}). We somewhat arbitrarily assume

that the tetragonal splitting within $^3T_{1g}(P)$ is the same as that within $^3T_{2g}(F)$, ~2000 cm^{-1}, so that average energies of these $^3T_{1,2g}$ states are easily calculated. This crude model yields Dq = 1394.4 cm^{-1} and B = 403.8 cm^{-1} (56.5% of the free-ion value[59]) which values can be compared to those for Ti^{II}:MgCl$_2$: Dq = 1018 cm^{-1} and B = 527 cm^{-1}.[50] and for *trans*-TiCl$_2$(py)$_4$: Dq = 1240 cm^{-1} and B = 477 cm^{-1}.[8] The general trend in Dq values is as expected in that the homoleptic hexachlorido complex gives the weakest field and the present, dichloridotetraamino complex gives the strongest, with the imino complex in between. The nephelauxetic effect (reduction in B from the free-ion value)[60] is larger for the N-donor complexes than for the pure halido species, as expected. However, the π-interacting py ligand might be expected to be more nephelauxetic than the σ-only tmeda, but this discrepancy might simply be due to the oversimplification of using a cubic model in these tetragonal cases. A tetragonal distortion can then be included (parameters Ds and Dt),[61] so that the observed band splitting can be modeled. The ground state is set to ^3E_g from $^3T_{1g}(F)$ in O_h symmetry, with $^3A_{2g}$ at arbitrary higher energy, as this would be far too low to be observed. We now directly include the tetragonal splitting within $^3T_{2g}(F)$: band 1 is the transition energy to $^3B_{2g}$, but we assume that band 2 alone represents the energy of ^3E_g, similar to what was done in the cubic symmetry case above. We further assume that the transition to $^3A_{2g}$ from $^3T_{1g}(P)$ in O_h symmetry is lower in energy than bands 4 and 5 (^3E_g from $^3T_{1g}(P)$), as assumed in the cubic case.[62] The fit parameters are (in cm^{-1}): Dq = 1499.0, Ds = −101.8, Dt = +260.5, and B = 427.2. These values are similar to those determined for *trans*-[TiCl$_2$(py)$_4$]: Dq = 1380, Ds = −462, Dt = +331, B = 439.4.[8] Jacobsen et al. determined a trigonal splitting for Ti^{II}:MgCl$_2$ given by Ds = 281 and Dt = −142,[50] which are similar magnitudes to our values and the change in sign is as expected for trigonal versus tetragonal distortion. Overall comparison among the three systems gives the same qualitative relationship as seen using only an octahedral crystal-field, with the nephelauxetic effect now being roughly the same (~60% of the free-ion value for B) for the two N-donor complexes, which is more satisfying than the result using only the cubic model.

With reasonable ligand-field parameters established based on spin-allowed (i.e., triplet−triplet) transitions, an estimate as to the Racah C parameter, which determines the singlet energies, can be used to explore spin-forbidden (i.e., triplet-singlet) transitions. With the above crystal-field (D_{4h} symmetry model: Dq, Ds, and Dt) and B parameters fixed, then the spin-forbidden band 3 to $^1A_{1g}$ (parent $^1A_{1g}(G,S)$ in O_h) can be exactly matched using C = 2328.5 cm^{-1} (87% of the free-ion value[59]).[63] These complete crystal-field model results are provided in Table S15, with detailed output from the Ligfield program[64] given in Table S16a. These results also show that the transition to $^3B_{1g}$ ($^3A_{2g}$ in O_h) would occur at 26 550 cm^{-1}, so there might be a d−d component to band 6, the lowest of the high-energy bands. The value for C is rather high for a covalent complex, and we have no explanation for this. The ratio C/B here equals 5.45, as opposed to 3.73 in the free-ion, which itself is relatively low for a 3d^n ion.[65] The chemical significance of interelectronic repulsion parameters, whether defined by the Slater−Condon or Racah formalisms, has been the subject of debate for many years.[60,66] Ferguson claimed that B and C reflect outer and inner electron shell properties, respectively, so that B becomes more reduced when going from the free ion to complexes, while C is reduced to a lesser extent.

Interelectronic repulsion parameters have been recently discussed by Singh et al. in the context of theoretical studies on $[MX_6]^{3\pm}$ complexes, where M = Cr^{III} and X = NH$_3$, F$^-$, Cl$^-$, Br$^-$, I$^-$, and CN$^-$, and where M = Mo^{III} and W^{III} and X = Cl$^-$.[67] Their calculations show a reduction in B in the order F$^-$, NH$_3$, Cl$^-$, Br$^-$, I$^-$, and CN$^-$, consistent with greater covalency, but the corresponding information for C is not provided. Clearly, more work is needed on a wider variety of ions, Cr^{III} being one of the few that have been extensively studied in this context,[66,67] so that the present results can be better understood.

To employ the AOM, we consider only σ-bonding for the tmeda N donors and the chlorido ligands are considered to be cylindrical π-donors, so there are three bonding parameters: $\varepsilon_{\sigma(N)}$, $\varepsilon_{\sigma(Cl)}$, and $\varepsilon_{\pi(Cl)}$. The Ti^{II} ion is on an inversion center in the current crystal structure (Figure 1), which makes the geometry well suited in principle to application of the AOM. We define the z axis as the Cl−Ti−Cl vector (∠Cl−Ti−Cl = 180.0°; ∠Cl−Ti−N = 90.0 ± 0.1°) and the x axis as bisecting the tmeda chelates.

This is shown in Scheme 1 and the resulting θ, φ angles for the AOM are given in Table S15. The deviation from ideal D_{4h}

Scheme 1. Structure of *trans*-[TiCl$_2$(tmeda)$_2$] for Application of AOM
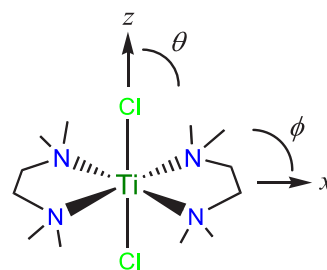
symmetry about the Ti^{II} ion is minimal;[68] so to facilitate the fitting, we begin with ideal D_{4h} symmetry ($\varphi = \pm 45°, \pm 135°$). A ^3E_g ground state obtains with a good fit to the bands derived from $^3T_{2g}$, but the relative energy of transitions involving $^3T_{1g}(P)$ must be reversed from that in the crystal-field model, i.e., $^3A_{2g}$ higher in energy than ^3E_g. Since the crystal-field fits have less connection (constraints due to) to molecular structure and bonding, and there is no solid experimental assignment to a transition to $^3A_{2g}(P)$, this reordering is not a concern. This fit gives the following bonding parameters (in cm^{-1}): $\varepsilon_{\sigma(N)}$ = 5185.4, $\varepsilon_{\sigma(Cl)}$ = 4010.1, $\varepsilon_{\pi(Cl)}$ = 345.4. In the previous study of *trans*-[TiCl$_2$(py)$_4$], π-interaction by the pyridine ligands was a complication, but estimates of $\varepsilon_{\sigma(N)}$ = 5000(100) and $\varepsilon_{\sigma(Cl)}$ = 3200(100) cm^{-1} were obtained,[8] which are consistent with those determined here for the tmeda complex. More generally, these AOM bonding parameters are in line with values for these types of donors.[69−72] For example, for *trans*-[CrCl$_2$(en)$_2$]$^+$ (in cm^{-1}): $\varepsilon_{\sigma(N)} \approx 7400$, $\varepsilon_{\sigma(Cl)} \approx 5700$, and $\varepsilon_{\pi(Cl)} \approx 1000$. Chromium(III) has stronger covalent and electrostatic interactions with these ligands than does titanium(II); therefore, the larger magnitudes of all of the bonding parameters of Cr^{III} are plausible. Early transition metals in low formal oxidation states are generally not the type of complex historically analyzed by classical LFT. A complex quite relevant to ours, namely Cs$_2$[*trans*-Ti^{III}Cl$_2$(H$_2$O)$_4$]Cl, was structurally characterized and studied by single crystal optical spectroscopy.[73] Disappointingly, attempts by these

workers to extract LFT parameters were unsuccessful. The homoleptic hexaaquavanadium(III) cation was successfully analyzed by the AOM to yield (in cm^{-1}) the following values: $\varepsilon_{\sigma(O)}$ = 6950, $\varepsilon_{\pi-\perp(O)}$ = 930, $\varepsilon_{\pi-\perp(O)}$ = 0.[74] These bonding parameters were also applicable to hexaaquatitanium(III).[75] The average π-bonding is similar to that seen here and stronger σ-bonding between H_2O and these 3+ cations is expected.

We can then successfully fit the spin-forbidden band 3, assigned as above using the crystal-field model, although a correspondingly large value for the Racah C parameter results (*vide supra*). The overall parameters are (in cm^{-1}) as follows: $\varepsilon_{\sigma(N)}$ = 5199.2, $\varepsilon_{\sigma(Cl)}$ = 3978.2, $\varepsilon_{\pi(Cl)}$ = 320.3, B = 454.8, and C = 2342.7, with the calculated energies given in Table S15.

Finally, we introduce the experimental D_{2h} symmetry. Although this allows the splitting between bands 4 and 5 more or less to be modeled, overall use of the slight structural difference between the x (inside chelate ring; see Scheme 1) and y (between the chelates) directions makes fitting the transitions derived from $^3T_{2g}(F)$ problematic. It is not possible to convert the generally successful D_{4h} AOM (*vide supra*) into one in D_{2h} symmetry that maintains the same bonding relationship, namely $\varepsilon_{\sigma(N)} > \varepsilon_{\sigma(Cl)}$. Clearly, all three components of the transitions derived from $^3T_{2g}(F)$, and possibly from $^3T_{1g}(P)$ as well, would have to have been observed for this method potentially to be viable. Moreover, the Ti-tmeda chelate ring may introduce distortions in bonding that are not manifest in the simple AOM used here. In Supporting Information, section S2 we provide an alternate AOM that is moderately successful in treating the experimental D_{2h} symmetry (see Tables S15 and S16b in particular), but it is less satisfactory in terms of the bonding parameters in that $\varepsilon_{\sigma(N)} < \varepsilon_{\sigma(Cl)}$.

The final potential application of LFT is to estimate the zfs. Jacobsen et al. did this successfully using the SOC coupling constant, ζ = 93 cm^{-1} (80% of the free-ion value[76]) which yielded D = +4.26 cm^{-1}, comparable to their experimental, axial value of D = +4.7 cm^{-1}.[50] The problem here is that, in contrast to the situation with Ti^{II}:MgCl$_2$, which had a $^3A_{2g}$ ground state (in D_{3d} symmetry), *trans*-[TiCl$_2$(tmeda)$_2$] has an orbitally degenerate ^3E_g ground state (in D_{4h} symmetry). This means that none of the LFT models successfully using this symmetry for the optical transitions can be then used for calculation of zfs for comparison with an S = 1 spin Hamiltonian.[8] Although the actual symmetry is indeed D_{2h} and the ground state is orbitally nondegenerate, one needs a fully successful AOM in this geometry, which is not the case. In Section S2, the alternate AOM is employed to calculate zfs with ambiguous results in that the magnitude of D can be reproduced, but not the sign (see Table S16c in particular). Fortunately, the quantum chemical theory (QCT) calculations, particularly those involving the *ab initio* approach, described in the following section, are successful in calculating the zfs in *trans*-[TiCl$_2$(tmeda)$_2$] using the actual molecular geometry.

Quantum Chemical Theory (QCT)—Geometry Optimizations. In order to better understand the spectroscopic properties and electronic structure of *trans*-[TiCl$_2$(tmeda)$_2$], we performed DFT and wave function-based (i.e., *ab initio*) computations. The majority of the computations were performed using the X-ray structure reported in this work, with the positions of the hydrogen atoms optimized using DFT. In addition, zfs parameters were calculated using two additional structures taken from (i) the previously reported XRD coordinates[13] and (ii) coordinates obtained from a full

DFT geometry optimization (*vide infra*). It is important to understand the impact of using DFT geometry-optimized models on calculated molecular properties, especially zfs parameters, as X-ray crystal structures are often unavailable for species of interest. It has been observed in some cases that the slight molecular deviations between crystallographic and DFT-derived structures significantly, and negatively, impact the agreement between experimental and calculated zfs parameters.[77]

Full geometry optimization of *trans*-[TiCl$_2$(tmeda)$_2$] using the BP functional (coordinates given in Tables S6 and S7), which is typically quite acceptable at reproducing experimental metal−ligand distances,[78] resulted in Ti−N bonds too long by 0.076 Å (this is not remedied by using a larger basis set). However, the Ti−Cl distance and metal−ligand bond angles were well reproduced (Table S14, which summarizes key metrics using multiple computational models). In an attempt to better reproduce the Ti−N bond lengths, geometry optimizations were performed using additional functionals (coordinates given in Tables S8−S11). While most functionals yielded models with Ti−N bond lengths overestimated by at least 0.08 Å, the geometry obtained using TPSSh-D3, a hybrid meta-GGA functional including dispersion corrections, showed very accurate Ti−N distances and Ti−Cl bond lengths only slightly too short (Tables 2 and S12). Thus, the TPSSh-D3 model was used in the calculation of zfs parameters, along with the models derived directly from the XRD coordinates.

Table 2. Bond Lengths (Å) and Bond Angles (deg) for *trans*-[TiCl$_2$(tmeda)$_2$] as Determined by X-ray Diffraction and DFT Energy Minimization Using the TPSSh-D3 Functional

|	experimental[a]	experimental[b]	TPSSh-D3
Ti−N	N1: 2.382(2)	N1: 2.381(7)	N1: 2.355
	N2: 2.376(2)	N2: 2.377(7)	N2: 2.362
Ti−Cl	2.5085(3)	2.477(2)	2.466
Cl1−Ti−Cl2	180.00	180.00(2)	180.00
Cl−Ti−N	N1: 90.03(3)	N1: 90.28(2)	N1: 87.82
	N1B: 89.97(3)	N1B: 89.72(2)	N1B: 92.27
	N2: 89.87(3)	N2: 89.98(2)	N2: 92.18
	N2B: 90.13(3)	N2B: 90.02(2)	N2B: 87.73
N1−Ti−N	N2: 79.13(4)	N2: 79.15(3)	N2: 80.30
	N1B: 180.00	N1B: 180.00(2)	N3: 180.00
	N2B: 259.13(4)	N2B: 259.15(2)	N4: 260.30

[a]Structure reported in this work (at 100 K). [b]Data taken from the structure reported by Edema et al. (at ambient temperature).[13]

Quantum Chemical Theory—Electronic Structure and Ligand-field Excited States. Spin unrestricted DFT computations using the present X-ray structure of *trans*-[TiCl$_2$(tmeda)$_2$] reveal a bonding description consistent with that presumed based on ligand-field theory considerations (Figure 4). Of the Ti^{II} 3d-based MOs, the 3d$_{xy}$ MO lies at lowest energy, as this is essentially a nonbonding MO. The near-degenerate Ti^{II} 3d$_{xz}$ and 3d$_{yz}$ MOs, which lie just above (α MOs), or interleave (β MOs), the 3d$_{xy}$ MO, are Ti−Cl π-antibonding, but show only a small admixture of Cl 3p character (Table 3 and Figure 8). These modest Ti−Cl π-interactions are consistent with the low $\varepsilon_{\pi(Cl)}$ parameter from the AOM analysis (*vide supra*). The calculated splitting of the 3d$_{xz}$ and 3d$_{yz}$ MOs is slight (0.52 eV or 4180 cm^{-1} for the (β MOs), but much larger than the 3d$_{xz}$-3d$_{yz}$ splitting

Table 3. Molecular Orbital Symmetry Labels, Energies (eV), and Percent Compositions Based on Spin Unrestricted DFT Computations for *trans*-[TiCl$_2$(tmeda)$_2$]

MO	symmetry label (in D_{2h})	occupancy	energy	% composition		
				Ti 3d[a]	Cl 3p + 3s[b]	N 2p + 2s[c]
93α	a$_g$(d$_{xy}$)	1.0	−3.2479	88.7	0.8	1.0
94α	b$_{2g}$(d$_{xz/yz}$)	1.0	−3.0188	89.2	7.8	0.4
95α	b$_{3g}$(d$_{yz/xz}$)	0.0	0.2562	91.4	4.2	0.4
99α	a$_g$(d$_{z^2}$)	0.0	1.7393	67.4	6.6	3.4
100α	b$_{1g}$(d$_{x^2-y^2}$)	0.0	1.7768	44.1	1.1	2.4
103α	b$_{1g}$(d$_{x2-y2}$)	0.0	2.1997	19.9	0.8	13.0
104α	b$_{1g}$(d$_{x^2-y^2}$)	0.0	2.2975	21.2	0.2	9.4
93β	a$_g$(d$_{xy}$)	0.0	0.8232	26.6	0.8	4.8
94β	b$_{3g}$(d$_{yz/xz}$)	0.0	1.0168	88.2	3.6	0.6
95β	a$_g$(d$_{xy}$)	0.0	1.1529	36.0	0.8	1.6
98β	b$_{2g}$(d$_{xz/yz}$)	0.0	1.5355	78.8	2.8	2.2
103β	a$_g$(dz^2)	0.0	2.4700	61.3	5.6	8.2
107β	b$_{1g}$(d$_{x^2-y^2}$)	0.0	2.7947	52.2	0.4	7.6

[a]Sum of all Ti 3d contributions to this MO. [b]Sum of all Cl 3p and 3s contributions to this MO. [c]Sum of all N 2p and 2s contributions to this MO.
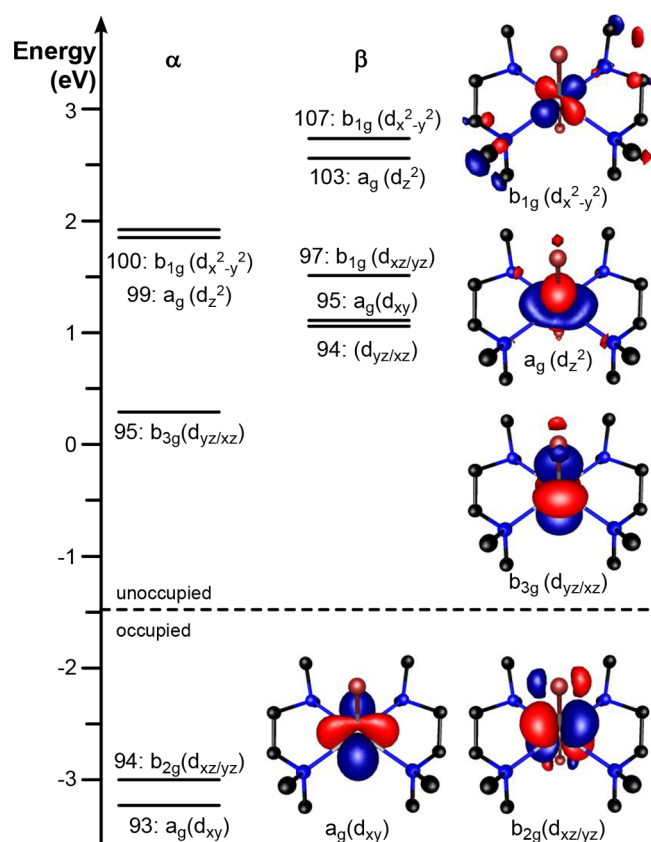
Figure 8. Ti 3d-orbital splitting pattern for *trans*-[TiCl$_2$(tmeda)$_2$] based on spin-unrestricted DFT calculations. Isosurface plots of the corresponding quasi-restricted MOs are included. The list of contributions to the Kohn−Sham orbitals is found in Table 3.

calculated for the related complex *trans*-[TiCl$_2$(py)$_4$] (0.12 eV or 970 cm^{-1}).[8] The metal−ligand metric parameters of the pyridine complex are much closer to that expected for a D_{4h} system, which accounts for the near-degeneracy of the 3d$_{xz}$ and 3d$_{yz}$ MOs in that case, and both the success and challenges of the LFT models (*vide supra*). For the tmeda complex, the e$_g$-derived 3d$_{x^2-y^2}$ and 3d$_{z^2}$ MOs are σ-antibonding with respect to the amine and chloride ligands, with 3d$_{x^2-y^2}$ at slightly higher energy (Table 3 and Figure 8). These results are qualitatively

the same as those from LFT, as can be seen from the MO descriptions of the ground state and selected triplet and singlet excited states given in Table S16, parts a (D_{4h} AOM) and b (D_{2h} AOM).

Using the molecular structure of *trans*-[TiCl$_2$(tmeda)$_2$], as derived by the XRD analysis at 100 K, electronic transition energies to all triplet and singlet excited states of the Ti^{II} center were calculated using the CASSCF/NEVPT2 method. This computational procedure offers a fairly economical and quite robust approach for calculating ground- and excited-state properties of transition metal complexes.[79−84] This method was previously used to examine the electronic transition energies and ground-state splitting of *trans*-[TiCl$_2$(py)$_4$].[8] Table 4 compares the CASSCF/NEVPT2 ligand-field excited-state energies with the transition energies determined by MCD spectroscopy. For clarity, we will compare experiment and theory using the parent O_h states.

The CASSCF/NEVPT2 computations predict the three components of the $^3T_{2g}$ excited state to fall in the range of 11 841 to 13 154 cm^{-1}. This prediction is in excellent agreement with the energies of MCD bands 1 and 2, which were attributed to excitations to the $^3T_{2g}$ excited state (Tables 1 and 4). The calculated energy of the $^1A_{1g}$ excited state (21 770 cm^{-1}) is in reasonable agreement with the energy of band 3 (16 825 cm^{-1}). The $^3T_{1g}$(P) excited state is calculated to have components from 20 012−23 407 cm^{-1}, in excellent agreement with the MCD pseudo-*A* term comprised of bands 4 and 5, which has positive and negative components at 18 750 and 19 050 cm^{-1} (Table 4). The highest-energy triplet excited state, $^3A_{2g}$, is calculated at 23 480 cm^{-1}, in reasonable agreement with MCD band 6 (28 550 cm^{-1}). Band 6 was not used in the LFT-based fits, but the transition to $^3A_{2g}$ was calculated to occur at ∼25 500 cm^{-1} using the optimal AOM (see Table S15), in further support of this assignment, although there could be a CT component as well. The high-energy UV bands 7 and 8 are difficult to assign. The optimal AOM fit affords spin-forbidden transitions to ^1E_g (in O_h, from free-ion ^1G and ^1D) at 30 000−31 000 cm^{-1} (see Table S15) so it is possible that these transitions might contribute to band 7. The highest energy band may be due to a CT transition, but its exact nature is unclear.

Electronic transition energies to all triplet and singlet excited states were also calculated using the multireference SORCI

Table 4. Energies (cm^{-1}) of Ligand-Field and Charge-Transfer States of *trans*-[TiCl$_2$(tmeda)$_2$] from Electronic Structure Computations and MCD Spectroscopy (XRD Crystal Structure Determined in This Work Used)

O_h parent states	D_{2h} states[a]	TD-DFT	NEVPT2	SORCI	MCD
$^3T_{1g}$(F)	$^3B_{2g}$	0	0	0	
	$^3B_{3g}$	3 457	1 237	1 177	
	$^3B_{1g}$	4 106	2 219	2 619	
$^1T_{2g}$	$^1B_{2g}$		8 992	9 253	
	^1A_g		9 221	9 669	
	^1A_g		10 384	10 784	
^1E_g	$^1B_{1g}$		11 482	12 616	
	^1A_g		11 912	12 957	
$^3T_{2g}$	^3A_g	13 154	11 841	11 162	11 560[b]
	$^3B_{3g}$	16 315	12 994	12 411	13 810
	$^3B_{2g}$	17 963	13 154	12 661	
$^1A_{1g}$	^1A_g		21 770	20 868	16 825
$^3T_{1g}$(P)	$^3B_{1g}$	19 198	20 012	19 218	
	$^3B_{3g}$	35 430	21 210	21 855	18 750
	$^3B_{2g}$	36 366	23 407	22 435	19 050
$^1T_{2g}$	^1A_g		22 490	22 507	
	$^1B_{3g}$		23 832	23 350	
	$^1B_{1g}$		24 671	23 432	
$^3A_{2g}$	$^3B_{1g}$	NA[b]	23 480	24 291	28 550[c]
$^1T_{1g}$	$^1B_{2g}$		25 117	24 166	
	$^1B_{2g}$		27 330	26 456	
	$^1B_{3g}$		27 817	26 718	
^1E_g	^1A_g		36 736	35 816	
	$^1B_{1g}$		36 748	35 962	
$^1A_{1g}$	^1A_g		47 744	40 031	

[a]The symmetry properties of the excited states were determined from the electronic configurations of the SORCI calculation or by analysis of the Kohn−Sham orbitals from the TD-DFT calculation. [b]The $^3A_{2g}$ excited state derives from a two-electron excitation. The TD-DFT method used here is unable to treat two-electron excited states. [c]The assignment of this feature is tentative. While we prefer its assignment as a charge transfer transition, it could instead derive from the $^3A_{2g}$ ligand-field excited state.

(*sp*ectroscopically *or*iented *c*onfiguration *i*nteraction) method, but employing the truncated model *trans*-[TiCl$_2$(eda)$_2$] (see Experimental Section). Although quite accurate, SORCI is economical for systems with small numbers of electrons,[41,85−90] so this modest truncation is worthwhile. The truncation of tmeda to eda is expected to impact only the energy of the 3d$_{x^2-y^2}$ MO, as the eda ligand should be a poorer σ-donor than tmeda. Consistent with this almost negligible effect, the CASSCF/NEVPT2 calculations for the eda and tmeda complexes show differences in transition energies typically less than 500 cm^{-1} (Supporting Information, Table S17). Likewise, the excited-state energies obtained from the SORCI calculation are in close agreement (generally within 1000 cm^{-1}) with those determined by the CASSCF/NEVPT2 method using the untruncated model (Table 4).

Given that the SORCI calculations for *trans*-[TiCl$_2$(eda)$_2$] properly reproduce the excited-state properties, it is warranted to discuss the ground-state bonding description afforded by this method. The multireference wave function in a SORCI calculation is composed of approximate average natural orbitals (AANOs), the advantages of which have been previously described.[41,89] The frontier AANOs of *trans*-[TiCl$_2$(eda)$_2$]

(Supporting Information, Figure S11) bear a close resemblance to frontier MOs (formally Kohn−Sham orbitals) of *trans*-[TiCl$_2$(tmeda)$_2$] in Figure 8. The SORCI calculations for *trans*-[TiCl$_2$(eda)$_2$] yield a $^3B_{2g}$ ground state (Table 4). The leading (85%) configuration in this state is (b$_{2g}$)^1(a$_g$)^1(b$_{3g}$)^0(a$_g$)^0(b$_{1g}$)^0 (Supporting Information, Table S18). Thus, the SORCI-computed ground-state has very little multiconfigurational character, and reinforces the bonding description obtained from the DFT computations and is also consistent with the simple LFT picture (Supporting Information, Table S16).

Finally, the time-dependent (TD) DFT method was employed to calculate electronic transition energies to triplet excited states of *trans*-[TiCl$_2$(tmeda)$_2$]. Although quite economical, TD-DFT is not always well-suited for calculating electronic transition energies for transition-metal complexes, especially when multiplet effects are involved.[78,91] Nonetheless, it is instructive to evaluate the efficacy of TD-DFT methods, as there are many instances where this approach performs laudably.[85,92,93] For *trans*-[TiCl$_2$(tmeda)$_2$], the energies of the $^3T_{2g}$ components at the TD-DFT level are overestimated compared to both experiment and the CASSCF/NEVPT2 and SORCI calculations (Table 4), but the deviation is modest ($\sim$2000−4000 cm^{-1}). In contrast, the components of the $^3T_{1g}$ excited state are in quite poor agreement, with the two higher-energy components predicted at >35 000 cm^{-1}, roughly 15 000 cm^{-1} higher than experiment (Table 4 and Supporting Information, Table S19). The reason for this large discrepancy is not clear and should be seen as a caveat to those who apply TD-DFT methods to seemingly tractable coordination complexes (i.e., a single 3d ion with ≤6 ligands from periods 2 and/or 3).

Quantum Chemical Theory—Ground-State Spin Hamiltonian Parameters. The calculation of zfs parameters for transition metal complexes using electronic structure methods remains a significant challenge.[77,83,94] However, both the CASSCF/NEVPT2[79−83] and SORCI[41,78,85−88] approaches have been shown to be rather reliable. In addition, several computational treatments of zfs can distinguish contributions from spin−orbit coupling (D_{SOC}) and spin−spin coupling (D_{SSC}). In many cases, but certainly not all,[88,95,96] D_{SSC} is quite small relative to D_{SOC}.

CASSCF/NEVPT2 calculations using the present XRD coordinates for *trans*-[TiCl$_2$(tmeda)$_2$] and an active space including the Ti^{II} 3d orbitals and electrons, CAS(2,5), yield D_{SOC} of −4.47 cm^{-1} and E/D of 0.21, in good agreement with the experimental values (D = −5.25(3) cm^{-1}, E/D = 0.165(3); combining the low and high temperature HFEPR values), assuming a small D_{SSC} contribution (*vide infra*). The g-values are also well-reproduced at this level of theory (Table 5). When CASSCF calculations lacking the dynamic correlation of the NEVPT2 approach are employed instead, the D_{SOC} value remains in good agreement with experimental data (D_{SOC} = −5.89 cm^{-1}), but the system is overly rhombic (E/D = 0.25), and the g-values are not as well predicted (Table 5). Thus, the NEVPT2 procedure improves the overall level of agreement at a fairly modest computational cost. Increasing the size of the active space to CAS(2,7) causes a 22% increase in the magnitude of D_{SOC} to −5.46 cm^{-1} and a decrease in E/D to 0.19, providing better agreement with experiment.

Given the success in the CASSCF/NEVPT2 approach in reproducing the zfs parameters, we investigated individual contributions to D_{SOC} and E_{SOC} from the ligand-field excited

Table 5. Calculated Ground-State Spin Hamiltonian Parameters D (cm^{-1}), $|E/D|$, and g-Values for *trans*-[TiCl$_2$((tm)eda)$_2$] Using Coordinates from the X-ray Structures and DFT Computations

Chelate	Method[a]	D_{tot}	D_{SOC}	D_{SSC}[b]	$|E/D|$	g[k]
tmeda	experiment[c]	−5.25(3)			0.165(3)	1.78(1), 1.88(2), 1.95(2)
			X-ray structure (this work)[d]			
tmeda	CAS(2,5)[e]		−5.89		0.25	1.719, 1.839, 1.948
tmeda	CAS(2,5)/NEVPT2[f]		−4.47		0.21	1.794, 1.893, 1.963
tmeda	CAS(2,7)[e]		−5.87		0.24	1.729, 1.849, 1.951
tmeda	CAS(2,7)/NEVPT2[f]		−5.46		0.19	1.763, 1.887, 1.960
eda[g]	CAS(2,5)/NEVPT2[f]		−4.76		0.16	1.792, 1.907, 1.961
eda[g]	SORCI[h]	−5.46	−5.93	0.51	0.11	
tmeda	CP-DFT	−1.93	−1.69	−0.24	0.21	1.946, 1.964, 1.988
			X-ray structure (Edema et al.)[13i]			
tmeda	CAS(2,5)/NEVPT2[f]		−4.54		0.18	1.798, 1.905, 1.964
			DFT-optimized (TPSSh-D3)[j]			
tmeda	CAS(2,5)/NEVPT2[f]		−4.63		0.17	1.798, 1.908, 1.965

[a]All calculations employed TZVP basis sets for Ti, N, and Cl and SVP basis sets for C and H. Increasing the basis sets size to TZVPP (Ti, N, and Cl) and TZVP (C and H) led to only a minor change in D (0.02 cm^{-1}) using the CAS(2,5) method. [b]Using *ORCA* 4.1.2, D_{SSC} = −0.35 cm^{-1} was calculated at the CAS(2,5)/NEVPT2 level using the X-ray structure of *trans*-[TiCl$_2$((tm)eda)$_2$] from this work. While the sign of the D_{SSC} contribution differs from that predicted by the SORCI methods, both computational approaches provide evidence that D_{SOC} is dominant for this system. [c]The values from fitting the HFEPR 2D (field vs frequency) 4−30 K data set are D = −5.23(1) cm^{-1}, E = −0.88(1) cm^{-1}, and g = [1.86(1), 1.94(2), 1.77(1)]). At 273 K, the parameters differ only slightly: D = −5.28(1) cm^{-1}, E = −0.857(5) cm^{-1}, and g = [1.891(2), 1.963(3), 1.786(3)]. The values in this table are an average of the two so as to accommodate the entire temperature range. The sign of D (with E given the same sign, by convention) was determined by VT HFEPR experiments. [d]The experimental structure reported in this work was used, with the positions of the hydrogen atoms optimized using DFT. The positions of all other atoms are from the X-ray structure coordinates. [e]All Ti^{II} 3d orbitals and electrons were in the active space. [f]The NEVPT2 method was used to incorporate dynamic correlation on top of a CASSCF calculation. [g]The truncated *trans*-[TiCl$_2$(eda)$_2$] system was generated by replacing the N-methyl groups with hydrogen atoms and DFT-optimizing the positions of all hydrogen atoms. [h]SORCI calculations employed a CAS(2,5) and ten triplet and 15 singlet roots. [i]The experimental structure reported by Edema and co-workers[13] (CSD code: KIKZUZ) was used, with the positions of the hydrogen atoms optimized using DFT. The positions of all other atoms are from the X-ray structure coordinates. [j]The tmeda complex was energy-minimized with respect to all nuclear coordinates in the absence of symmetry constraints. [k]The g values are listed in order simply as g_{min}, g_{mid}, g_{max}, rather than with assignments in the molecular frame (g_x, g_y, g_z) as from the EPR simulations.

states. These results are displayed in the Supporting Information (Table S20). The dominant contributions to the Ti^{II} zfs arise from the $^3B_{3g}$ and $^3B_{1g}$ components of the $^3T_{1g}$(F) ground state (Figure 4). These excited states are calculated at 1237 and 2219 cm^{-1} above the $^3B_{2g}$ ground state (Table 4) and contribute −5.61 and +1.49 cm^{-1} to D_{SOC} (Table S20). The $^3B_{1g}$ state also makes a sizable contribution to E_{SOC} (−1.46 cm^{-1}), which can account in large part for the rhombicity seen by HFEPR for *trans*-[TiCl$_2$(tmeda)$_2$]. The five components of the low-lying $^1T_{1g}$ and ^1E_g excited states make contributions to D_{SOC} of similar magnitude, but of opposite sign (0.337 and −0.453 cm^{-1}, respectively), netting only a small overall impact. The components of the $^3T_{2g}$ excited state also provide modest contributions to D_{SOC} and E_{SOC} (−0.385 and 0.377 cm^{-1}, respectively). All other excited states make only slight contributions to the overall zfs (Supporting Information, Table S20).

The CASSCF/NEVPT2 zfs parameters do not vary significantly as a function of the *trans*-[TiCl$_2$(tmeda)$_2$] model (Table 5). Separate calculations using the X-ray coordinates from Edema et al.[13] and the coordinates obtained from a DFT geometry optimization yield D_{SOC} of −4.54 and −4.63 cm^{-1}, respectively (Table 5). In addition, CASSCF/NEVPT2 calculations using the truncated *trans*-[TiCl$_2$(eda)$_2$] model yield zfs parameters similar to those of the untruncated model (Table 5).

The SORCI calculations for the truncated system also accurately reproduce the experimental zfs parameters of *trans*-[TiCl$_2$(eda)$_2$]. The calculated D value of −5.46 cm^{-1} is within 3% of the experimental value, although $|E/D|$ is calculated to

be too small (0.11 versus 0.16 experimentally). D_{SOC} and D_{SSC} contributions calculated by the SORCI method show the latter to contribute only 10% of the total D value of *trans*-[TiCl$_2$(eda)$_2$] (Supporting Information, Table S21). With regard to D_{SOC}, the dominant contributions come from the lowest-energy $^3B_{3g}$ and $^3B_{1g}$ states, fully consistent with the CASSCF/NEVPT2 results for *trans*-[TiCl$_2$(tmeda)$_2$].

We note for completeness that CP-DFT calculations performed for the X-ray model of *trans*-[TiCl$_2$(eda)$_2$] properly reproduce the sign of D (i.e., D < 0 cm^{-1}), but the magnitude of D (−1.93 cm^{-1}) is in error by ∼60%. The calculated g-values are also too large (Table 5). We screened several different functionals in an effort to improve upon the agreement between experiment and theory (Supporting Information, Table S22). An improvement in the magnitude of D was only observed using the hybrid M06 functional (D = −2.58 cm^{-1}), but, again, the system was overly rhombic (E/D = 0.28). All pure functionals (BP, TPSS, and M06-L) yielded D > 0 cm^{-1}, in clear disagreement with the experimental result (albeit consistent with LFT). Finally, the CP-DFT-calculated zfs parameters show more variability as a function of the model geometry (Supporting Information, Table S21). For example, the B3LYP-calculated $|E/D|$ values range from 0.10, using the coordinates of the XRD structure of Edema and co-workers,[13] to 0.32 when the DFT-optimized coordinates are used (Supporting Information, Table S21).

■ CONCLUSIONS

A relatively rare example of a stable Ti^{II} coordination complex is *trans*-[TiCl$_2$(tmeda)$_2$], which was first reported many years

ago.[13] This complex comprises innocent ligands and is thus a *bona fide* example of Ti[II]. The Ti[II] ion is also unambiguously found in solid state chemistry, namely as a dopant into ionic solids (MgX_2, X = Cl, Br).[50,57] The optical spectroscopy of the Ti[II] dopant was thoroughly investigated, but corresponding studies on molecular complexes of Ti[II] are limited to the complex *trans*-[$TiCl_2(py)_4$],[8] which has an orbitally degenerate ground state, unlike the Ti[II] dopant. We have therefore brought back *trans*-[$TiCl_2(tmeda)_2$], including a redetermination of its single crystal XRD structure, this time at low temperature (100 K) and applying optical spectroscopy to the complex, in the form of VTVH-MCD. We have also applied techniques closely related to VTVH-MCD, namely dc magnetometry and paramagnetic resonance, in the form of HFEPR, to this orbitally nondegenerate $S = 1$ complex so that its spin Hamiltonian parameters (zfs and g-values) were accurately determined. All of this spectroscopic/physical information was then combined with theory, in the form of both classical LFT and the latest QCT methods (both DFT and *ab initio*). The result is a complete picture of the electronic structure of the Ti[II] ion in this relatively simple ligand environment, in terms of being nearly tetragonally symmetric (D_{4h}) with σ-only equatorial donors and cylindrical axial π-donors. The bidentate tmeda chelate has a crucial role in reducing the effective symmetry to D_{2h} so that the degeneracy of the d_{xz} and d_{yz} orbitals is removed, making the ground state $^3B_{2g}$, as opposed to ^3E_g in *trans*-[$TiCl_2(py)_4$].[8] The higher symmetry of *trans*-[$TiCl_2(py)_4$] gives rise to the unusual magnetic properties of this complex, as exemplified by a D of $-60(5)$ cm^{-1}, when using a spin Hamiltonian approach (however, in such cases where D is exceptionally large, a spin Hamiltonian approach is not appropriate; see the discussion in Wijeratne et al.[8]). In contrast, *trans*-[$TiCl_2(tmeda)_2$] has a more "conventional" D of $-5.25(3)$ cm^{-1} and is well described by a spin Hamiltonian model. The d orbital energies in *trans*-[$TiCl_2(tmeda)_2$] are well-determined by the combination of experiment and theory. This concord between experiment and theory is gratifying, but is expected for this Ti[II] complex with relatively high symmetry and "simple" ligands that are ubiquitous in coordination chemistry. Therefore, it is sobering that it was a challenge to reproduce the ground-state spin Hamiltonian parameters for this complex. Both CP-DFT methods and AOM approaches were less than satisfactory in predicting zfs parameters, while the *ab initio* CASSCF/NEVPT2 and SORCI methods performed laudably. The degree of understanding of electronic structure of a reduced, early transition metal complex, in a high spin ground state that we now have for *trans*-[$TiCl_2(tmeda)_2$] makes this complex a benchmark for future investigation of more reactive complexes of Ti[II] and other low oxidation state, paramagnetic early transition metal ions. In particular, the *trans*-[$TiX_2(dmpe)_2$] series (X = halide), along with their V[II] ($3d^3$) and Cr[II] ($3d^4$) congeners,[9] respectively, with spin quartet and triplet ground states, will be the subject of future studies.

ASSOCIATED CONTENT

SI Supporting Information

The Supporting Information is available free of charge at https://pubs.acs.org/doi/10.1021/acs.inorgchem.0c00311.

Additional MCD spectra, magnetometry plots, and HFEPR spectra, additional discussion of XRD results

and LFT analysis, and tables of results from LFT and QCT calculations (PDF)

Accession Codes

CCDC 1907543 contains the supplementary crystallographic data for this paper. These data can be obtained free of charge via www.ccdc.cam.ac.uk/data_request/cif, or by emailing data_request@ccdc.cam.ac.uk, or by contacting The Cambridge Crystallographic Data Centre, 12 Union Road, Cambridge CB2 1EZ, UK; fax: +44 1223 336033.

■ AUTHOR INFORMATION

Corresponding Authors

Timothy A. Jackson − *Department of Chemistry, University of Kansas, Lawrence, Kansas 66045, United States;* ● orcid.org/0000-0002-3529-2715; Email: taj@ku.edu

Joshua Telser − *Department of Biological, Physical and Health Sciences, Roosevelt University, Chicago, Illinois 60605, United States;* ● orcid.org/0000-0003-3307-2556; Email: jtelser@roosevelt.edu

Authors

Eva M. Zolnhofer − *Department of Chemistry and Pharmacy, Inorganic Chemistry, Friedrich-Alexander University Erlangen-Nürnberg (FAU), 91058 Erlangen, Germany*

Gayan B. Wijeratne − *Department of Chemistry, University of Kansas, Lawrence, Kansas 66045, United States;* ● orcid.org/0000-0001-7609-6406

Skye Fortier − *Department of Chemistry and Molecular Structure Center, Indiana University, Bloomington, Indiana 47405, United States;* ● orcid.org/0000-0002-0502-5229

Frank W. Heinemann − *Department of Chemistry and Pharmacy, Inorganic Chemistry, Friedrich-Alexander University Erlangen-Nürnberg (FAU), 91058 Erlangen, Germany;* ● orcid.org/0000-0002-9007-8404

Karsten Meyer − *Department of Chemistry and Pharmacy, Inorganic Chemistry, Friedrich-Alexander University Erlangen-Nürnberg (FAU), 91058 Erlangen, Germany;* ● orcid.org/0000-0002-7844-2998

J. Krzystek − *National High Magnetic Field Laboratory, Florida State University, Tallahassee, Florida 32310, United States;* ● orcid.org/0000-0001-6088-1936

Andrew Ozarowski − *National High Magnetic Field Laboratory, Florida State University, Tallahassee, Florida 32310, United States;* ● orcid.org/0000-0001-6225-9796

Daniel J. Mindiola − *Department of Chemistry, University of Pennsylvania, Philadelphia, Pennsylvania 19104, United States;* ● orcid.org/0000-0001-8205-7868

Complete contact information is available at:
https://pubs.acs.org/10.1021/acs.inorgchem.0c00311

Notes

The authors declare no competing financial interest.

■ REFERENCES

(1) Chirik, P. J. Group 4 Transition Metal Sandwich Complexes: Still Fresh after Almost 60 Years. *Organometallics* **2010**, *29*, 1500−1517.

(2) Troyanov, S. I.; Antropiusová, H.; Mach, K. Direct proof of the molecular structure of dimeric titanocene; The X-ray structure of $\mu(\eta^5{:}\eta^5$-fulvalene)-di-(μ-hydrido)-bis(η^5-cyclopentadienyltitanium)· 1.5 benzene. *J. Organomet. Chem.* **1992**, *427*, 49−55.

(3) Lukešová, L.; Horáček, M.; Štěpnička, P.; Fejfarová, K.; Gyepes, R.; Císařová, I.; Kubišta, J.; Mach, K. Synthesis and crystal structures of thermally stable titanocenes. *J. Organomet. Chem.* **2002**, *663*, 134−144.

(4) Fowles, G. W. A.; Lester, T. E.; Walton, R. A. Co-ordination complexes of titanium(II). *J. Chem. Soc. A* **1968**, 1081−1085.

(5) Calderazzo, F.; De Benedetto, G. E.; Engler, U.; Ferri, I.; Pampaloni, G.; Wagner, T. New preparative methods for the halides of titanium(II) and vanadium(II). Reduction of titanium(IV) halides with sodium and oxidation of bis(mesitylene)vanadium(0). *Z. Naturforsch., B* **1996**, *51*, 506−516.

(6) Kölle, U.; Kölle, P. Aqueous Chemistry of Titanium(II) Species. *Angew. Chem., Int. Ed.* **2003**, *42*, 4540−4542.

(7) Araya, M. A.; Cotton, F. A.; Matonic, J. H.; Murillo, C. A. An Efficient Reduction Process Leading to Titanium(II) and Niobium-(II): Preparation and Structural Characterization of *trans*-MCl$_2$(py)$_4$ Compounds, M = Ti, Nb, and Mn. *Inorg. Chem.* **1995**, *34*, 5424−5428.

(8) Wijeratne, G. B.; Zolnhofer, E. M.; Fortier, S.; Grant, L. N.; Carroll, P. J.; Chen, C.-H.; Meyer, K.; Krzystek, J.; Ozarowski, A.; Jackson, T. A.; Mindiola, D. J.; Telser, J. Electronic Structure and Reactivity of a Well-Defined Mononuclear Complex of Ti(II). *Inorg. Chem.* **2015**, *54*, 10380−10397.

(9) Girolami, G. S.; Wilkinson, G.; Galas, A. M. R.; Thornton-Pett, M.; Hursthouse, M. B. Synthesis and properties of the divalent 1,2-bis(dimethylphosphino)ethane (dmpe) complexes MCl$_2$(dmpe)$_2$ and MMe$_2$(dmpe)$_2$ (M = Ti, V, Cr, Mn, or Fe). X-Ray crystal structures of MCl$_2$(dmpe)$_2$ (M = Ti, V, or Cr), MnBr$_2$(dmpe)$_2$, TiMe$_{1.3}$Cl$_{0.7}$(dmpe)$_2$, and CrMe$_2$(dmpe)$_2$. *J. Chem. Soc., Dalton Trans.* **1985**, 1339−1348.

(10) Jensen, J. A.; Wilson, S. R.; Schultz, A. J.; Girolami, G. S. Divalent titanium chemistry. Synthesis, reactivity, and x-ray and neutron diffraction studies of Ti(BH$_4$)$_2$(dmpe)$_2$ and Ti-(CH$_3$)$_2$(dmpe)$_2$. *J. Am. Chem. Soc.* **1987**, *109*, 8094−8096.

(11) Jensen, J. A.; Girolami, G. S. Synthesis, characterization, and x-ray crystal structures of the divalent titanium complex Ti(η^2-BH$_4$)$_2$(dmpe)$_2$ and the unidentate tetrahydroborate complex V(η^1-BH$_4$)$_2$(dmpe)$_2$. *Inorg. Chem.* **1989**, *28*, 2107−2113.

(12) Morris, R. J.; Girolami, G. S. On the 1-donor ability of early transition metals: evidence that trialkylphosphines can engage in –back-bonding and x-ray structure of the titanium(II) phenoxide Ti(OPh)$_2$(dmpe)$_2$. *Inorg. Chem.* **1990**, *29*, 4167−4169.

(13) Edema, J. J. H.; Duchateau, R.; Gambarotta, S.; Hynes, R.; Gabe, E. Novel titanium(II) amine complexes L$_4$TiCl$_2$ [L = 1/2 *NNN′,N′*-tetramethylethylenediamine (TMEDA), 1/2 *NNN′*-trimethylethylenediamine, pyridine, 1/2 2,2′-bipyridine]: synthesis and crystal structure of monomeric *trans*-(TMEDA)$_2$TiCl$_2$. *Inorg. Chem.* **1991**, *30*, 154−156.

(14) Edema, J. J. H.; Gambarotta, S.; Duchateau, R.; Bensimon, C. Labile triangulo-trititanium(II) and trivanadium(II) clusters. *Inorg. Chem.* **1991**, *30*, 3585−3587.

(15) Duchateau, R.; Gambarotta, S.; Beydoun, N.; Bensimon, C. Side-on versus end-on coordination of dinitrogen to titanium(II) and mixed-valence titanium(I)/titanium(II) amido complexes. *J. Am. Chem. Soc.* **1991**, *113*, 8986−8988.

(16) Duchateau, R.; Williams, A. J.; Gambarotta, S.; Chiang, M. Y. Carbon-carbon double-bond formation in the intermolecular acetonitrile reductive coupling promoted by a mononuclear titanium-(II) compound. Preparation and characterization of two titanium(IV) imido derivatives. *Inorg. Chem.* **1991**, *30*, 4863−4866.

(17) Manxzer, L. E.; Deaton, J.; Sharp, P.; Schrock, R. R. Tetrahydrofuran Complexes of Selected Early Transition Metals. *Inorg. Synth.* **2007**, *21*, 135−140.

(18) Bain, G. A.; Berry, J. F. Diamagnetic Corrections and Pascal's Constants. *J. Chem. Educ.* **2008**, *85*, 532−536.

(19) Neese, F.; Solomon, E. I. MCD *C*-Term Signs, Saturation Behavior, and Determination of Band Polarizations in Randomly Oriented Systems with Spin $S \geq 1/2$. Applications to $S = 1/2$ and $S = 5/2$. *Inorg. Chem.* **1999**, *38*, 1847−1865.

(20) Hassan, A. K.; Pardi, L. A.; Krzystek, J.; Sienkiewicz, A.; Goy, P.; Rohrer, M.; Brunel, L.-C. Ultrawide band multifrequency high-field EMR technique: a methodology for increasing spectroscopic information. *J. Magn. Reson.* **2000**, *142*, 300−312.

(21) Neese, F. *ORCA - an ab initio, Density Functional and Semiempirical Program Package*, Version 3.0; Max Planck Institute for Chemical Energy Conversion: 2013.

(22) Neese, F. The ORCA program system. *Wiley Interdiscip. Rev.: Comput. Mol. Sci.* **2012**, *2*, 73−78.

(23) Becke, A. D. Density Functional Calculations of Molecular Bond Energies. *J. Chem. Phys.* **1986**, *84*, 4524−4529.

(24) Perdew, J. P. Density-functional approximation for the correlation energy of the inhomogeneous electron gas. *Phys. Rev. B: Condens. Matter Mater. Phys.* **1986**, *33*, 8822−8824.

(25) Schäfer, A.; Horn, H.; Ahlrichs, R. Fully optimized contracted Gaussian basis sets for atoms Li to Kr. *J. Chem. Phys.* **1992**, *97*, 2571−2577.

(26) Schäfer, A.; Huber, C.; Ahlrichs, R. Fully Optimized Contracted Gaussian Basis Sets of Triple Zeta Valence Quality for Atoms Li to Kr. *J. Chem. Phys.* **1994**, *100*, 5829−5835.

(27) Becke, A. D. Density-functional Thermochemistry. III. The Role of Exact Exchange. *J. Chem. Phys.* **1993**, *98*, 5648−5652.

(28) Becke, A. D. A New Mixing of Hartree-Fock and Local-density-functional Theories. *J. Chem. Phys.* **1993**, *98*, 1372−1377.

(29) Lee, C.; Yang, W.; Parr, R. G. Development of the Colle-Salvetti Correlation-energy Formula into a Functional of the Electron Density. *Phys. Rev. B: Condens. Matter Mater. Phys.* **1988**, *37*, 785−789.

(30) Grimme, S.; Antony, J.; Ehrlich, S.; Krieg, H. A consistent and accurate ab initio parametrization of density functional dispersion correction (DFT-D) for the 94 elements H-Pu. *J. Chem. Phys.* **2010**, *132*, 154104.

(31) Grimme, S.; Ehrlich, S.; Goerigk, L. Effect of the damping function in dispersion corrected density functional theory. *J. Comput. Chem.* **2011**, *32*, 1456−1465.

(32) Ekström, U.; Visscher, L.; Bast, R.; Thorvaldsen, A. J.; Ruud, K. Arbitrary-Order Density Functional Response Theory from Automatic Differentiation. *J. Chem. Theory Comput.* **2010**, *6*, 1971−1980.

(33) Zhao, Y.; Truhlar, D. G. Density Functionals with Broad Applicability in Chemistry. *Acc. Chem. Res.* **2008**, *41*, 157−167.

(34) Zhao, Y.; Truhlar, D. G. The M06 suite of density functionals for main group thermochemistry, thermochemical kinetics, non-covalent interactions, excited states, and transition elements: two new functionals and systematic testing of four M06-class functionals and 12 other functionals. *Theor. Chem. Acc.* **2008**, *120*, 215−241.

(35) Tao, J.; Perdew, J. P.; Staroverov, V. N.; Scuseria, G. E. Climbing the Density Functional Ladder: Nonempirical Meta-Generalized Gradient Approximation Designed for Molecules and Solids. *Phys. Rev. Lett.* **2003**, *91*, 146401.

(36) Schäfer, A.; Horn, H.; Ahlrichs, R. Fully Optimized Contracted Gaussian Basis Sets for Atoms Lithium to Krypton. *J. Chem. Phys.* **1992**, *97*, 2571−2577.

(37) Weigend, F.; Ahlrichs, R. Balanced basis sets of split valence, triple zeta valence and quadruple zeta valence quality for H to Rn:

Design and assessment of accuracy. *Phys. Chem. Chem. Phys.* **2005**, *7*, 3297−3305.

(38) Neese, F. An Improvement of the Resolution of the Identity Approximation for the Calculation of the Coulomb Matrix. *J. Comput. Chem.* **2003**, *24*, 1740−1747.

(39) Neese, F.; Wennmohs, F.; Hansen, A.; Becker, U. Efficient, approximate and parallel Hartree-Fock and hybrid DFT calculations. A 'chain-of-spheres' algorithm for the Hartree-Fock exchange. *Chem. Phys.* **2009**, *356*, 98−109.

(40) Angeli, C.; Cimiraglia, R.; Evangelisti, S.; Leininger, T.; Malrieu, J.-P. Introduction of n-electron valence states for multi-reference perturbation theory. *J. Chem. Phys.* **2001**, *114*, 10252−10264.

(41) Neese, F. A spectroscopy oriented configuration interaction procedure. *J. Chem. Phys.* **2003**, *119*, 9428−9443.

(42) Neese, F. Calculation of the zero-field splitting tensor on the basis of hybrid density functional and Hartree-Fock theory. *J. Chem. Phys.* **2007**, *127*, 164112.

(43) Hirata, S.; Head-Gordon, M. Time-dependent Density Functional Theory within the Tamm-Dancoff Approximation. *Chem. Phys. Lett.* **1999**, *314*, 291−299.

(44) Hirata, S.; Head-Gordon, M. Time-dependent Density Functional Theory for Radicals: An Improved Description of Excited States with Substantial Double Excitation Character. *Chem. Phys. Lett.* **1999**, *302*, 375−382.

(45) Casida, M. E.; Jamorski, C.; Casida, K. C.; Salahub, D. R. Molecular Excitation Energies to High-lying bound States from Time-dependent Density-functional Response Theory: Characterization and Correction of the Time-dependent Local Density Approximation Ionization Threshold. *J. Chem. Phys.* **1998**, *108*, 4439−4449.

(46) Bauernschmitt, R.; Ahlrichs, R. Treatment of electronic excitations within the adiabatic approximation of time dependent density functional theory. *Chem. Phys. Lett.* **1996**, *256*, 454−464.

(47) The stability of the complex in solvents in which it is sufficiently soluble (e.g., THF) is too low to allow collection of reliable solution MCD or even electronic absorption spectra.

(48) Kirk, M. L.; Peariso, K. Recent Applications of MCD Spectroscopy to Metalloenzymes. *Curr. Opin. Chem. Biol.* **2003**, *7*, 220−227.

(49) Piepho, S. B.; Schatz, P. N. *Group Theory in Spectroscopy with Applications to Magnetic Circular Dichroism*; Wiley: New York, 1983.

(50) Jacobsen, S. M.; Güdel, H. U.; Daul, C. A. Excited States of Titanium (2+): Sharp-Band and Broad-Band Near-Infrared Luminescence from Ti^{2+} in MgCl$_2$ and MgBr$_2$. *J. Am. Chem. Soc.* **1988**, *110*, 7610−7616.

(51) Solomon, E. I. Basic Principles and the Experiment: Electronic Absorption-Charge Transfer Transitions. *Comments Inorg. Chem.* **1984**, *3*, 249−260.

(52) Solomon, E. I.; Lever, A. B. P. *Inorganic Electronic Structure and Spectroscopy*; Wiley: New York, 1999.

(53) Boča, R. Zero-field splitting in metal complexes. *Coord. Chem. Rev.* **2004**, *248*, 757−815.

(54) Telser, J.; Pardi, L. A.; Krzystek, J.; Brunel, L.-C. EPR spectra from 'EPR-silent' species: high-field EPR spectroscopy of aqueous chromium(II). *Inorg. Chem.* **1998**, *37*, 5769−5775.

(55) Krzystek, J.; Ozarowski, A.; Telser, J. Multi-frequency, high-field EPR as a powerful tool to accurately determine zero-field splitting in high-spin transition metal coordination complexes. *Coord. Chem. Rev.* **2006**, *250*, 2308−2324.

(56) Krzystek, J.; Zvyagin, S. A.; Ozarowski, A.; Trofimenko, S.; Telser, J. Tunable-frequency high-field electron paramagnetic resonance. *J. Magn. Reson.* **2006**, *178*, 174−183.

(57) Wenger, O. S.; Güdel, H. U. Influence of Crystal Field Parameters on Near-Infrared to Visible Photon Upconversion in Ti^{2+} and Ni^{2+} Doped Halide Lattices. *Struct. Bonding* **2004**, *106*, 59−70.

(58) Schäffer, C. E. A Perturbation Representation of Weak Covalent Bonding. *Struct. Bonding (Berlin)* **1968**, *5*, 68−95.

(59) Brorson, M.; Schäffer, C. E. Orthonormal interelectronic repulsion operators in the parametrical d^q model. Application of the model to gaseous ions. *Inorg. Chem.* **1988**, *27*, 2522−2530.

(60) Jørgensen, C. K. The Nephelauxetic Series. *Prog. Inorg. Chem.* **2007**, *4*, 73−124.

(61) Ballhausen, C. J. In *Introduction to Ligand Field Theory*; McGraw-Hill: New York, 1962; pp 99−103.

(62) If $^3A_{2g}$ is placed higher in energy than ^3E_g, then the fits try to eliminate any tetragonal splitting within $^3T_{1g}(P)$ with overall unsatisfactory results.

(63) Jacobsen et al.[50] observed a single, spin-forbidden emission at 7 664.6 cm^{-1} that led to their use of $C = 1983$ cm^{-1} (74% of the free-ion value). The only viable assignment of band 3 to another singlet state is to $^1B_{1g}$ (which is ^1A_g in D_{2h} and has parent $^1T_{2g}(G,D)$ in O_h) requires an unacceptably low value of $C = 789$ cm^{-1}.

(64) Bendix, J. Ligfield. *Comprehensive Coordination Chemistry II, Volume 2: Fundamentals: Physical Methods, Theoretical Analysis, and Case Studies* **2003**, *2*, 673−676.

(65) The average of C/B we calculate for all 3d^n configurations for which these parameters are readily available[59] equals 4.12.

(66) Ferguson, J.; Wood, D. L. Crystal field spectra of d^{3,7} ions. VI. The weak field formalism and covalency. *Aust. J. Chem.* **1970**, *23*, 861−871.

(67) Singh, S. K.; Eng, J.; Atanasov, M.; Neese, F. Covalency and chemical bonding in transition metal complexes: An ab initio based ligand field perspective. *Coord. Chem. Rev.* **2017**, *344*, 2−25.

(68) The chelate ∠N−Ti−N is 79.1° (so the nonchelate ∠N−Ti−N is 101.9°); thus the deviation from ideal 4-fold symmetry for each ϕ angle is ∼ ± 5°: $\phi = \pm40°$ and $\pm140°$.

(69) Miessler, G. L.; Fischer, P. J.; Tarr, D. A. *Inorganic Chemistry*, 5th ed.; Pearson: Upper Saddle River, NJ, 2014.

(70) Figgis, B. N.; Hitchman, M. A. *Ligand Field Theory and its Applications*; Wiley-VCH: New York, 2000.

(71) Bridgeman, A. J.; Gerloch, M. The Interpretation of Ligand Field Parameters. *Prog. Inorg. Chem.* **2007**, *45*, 179−281.

(72) Gerloch, M.; Slade, R. C. In *Ligand-Field Parameters*; Cambridge University Press: Cambridge, U.K., 1973.

(73) McCarthy, P. J.; Lauffenburger, J. C.; Schreiner, M. M.; Rohrer, D. C. Crystal structure, low-temperature crystal spectra and IR spectra of tricesium dichlorotetraaquavanadium(III) chloride and some analogous molecules. *Inorg. Chem.* **1981**, *20*, 1571−1576.

(74) Tregenna-Piggott, P. L. W.; Best, S. P.; Güdel, H. U.; Weihe, H.; Wilson, C. C. Influence of the Mode of Water Coordination on the Electronic Structure of the $[V(OH_2)_6]^{3+}$ Cation. *J. Solid State Chem.* **1999**, *145*, 460−470.

(75) Tregenna-Piggott, P. L. W.; Andres, H.-P.; McIntyre, G. J.; Best, S. P.; Wilson, C. C.; Cowan, J. A. Aqua ions. 2. Structural manifestations of the Jahn-Teller effect in the C-alums. *Inorg. Chem.* **2003**, *42*, 1350−1365.

(76) Bendix, J.; Brorson, M.; Schäffer, C. E. Accurate empirical spin orbit coupling parameters z$_{nd}$ for gaseous nd^q transition metal ions. The parametrical multiplet term model. *Inorg. Chem.* **1993**, *32*, 2838−2849.

(77) Zein, S.; Duboc, C.; Lubitz, W.; Neese, F. A Systematic Density Functional Study of the Zero-Field Splitting in Mn(II) Coordination Compounds. *Inorg. Chem.* **2008**, *47*, 134−142.

(78) Neese, F. A critical evaluation of DFT, including time-dependent DFT, applied to bioinorganic chemistry. *JBIC, J. Biol. Inorg. Chem.* **2006**, *11*, 702−711.

(79) Duboc, C.; Ganyushin, D.; Sivalingam, K.; Collomb, M.-N.; Neese, F. Systematic Theoretical Study of the Zero-Field Splitting in Coordination Complexes of Mn(III). Density Functional Theory versus Multireference Wave Function Approaches. *J. Phys. Chem. A* **2010**, *114*, 10750−10758.

(80) Zadrozny, J. M.; Atanasov, M.; Bryan, A. M.; Lin, C.-Y.; Rekken, B. D.; Power, P. P.; Neese, F.; Long, J. R. Slow magnetization dynamics in a series of two-coordinate iron(II) complexes. *Chem. Sci.* **2013**, *4*, 125−138.

(81) Atanasov, M.; Zadrozny, J. M.; Long, J. R.; Neese, F. A theoretical analysis of chemical bonding, vibronic coupling, and magnetic anisotropy in linear iron(II) complexes with single-molecule magnet behavior. *Chem. Sci.* **2013**, *4*, 139−156.

(82) Atanasov, M.; Ganyushin, D.; Pantazis, D. A.; Sivalingam, K.; Neese, F. Detailed Ab Initio First-Principles Study of the Magnetic Anisotropy in a Family of Trigonal Pyramidal Iron(II) Pyrrolide Complexes. *Inorg. Chem.* **2011**, *50*, 7460−7477.

(83) Maganas, D.; Krzystek, J.; Ferentinos, E.; Whyte, A. M.; Robertson, N.; Psycharis, V.; Terzis, A.; Neese, F.; Kyritsis, P. Investigating Magnetostructural Correlations in the Pseudooctahedral trans-[Ni^{II}{(OPPh$_2$)(EPPh$_2$)N}$_2$(sol)$_2$] Complexes (E = S, Se; sol = DMF, THF) by Magnetometry, HFEPR, and ab initio Quantum Chemistry. *Inorg. Chem.* **2012**, *51*, 7218−7231.

(84) Colmer, H. E.; Geiger, R. A.; Leto, D. F.; Wijeratne, G. B.; Day, V. W.; Jackson, T. A. Geometric and electronic structure of a peroxomanganese(III) complex supported by a scorpionate ligand. *Dalton Trans.* **2014**, *43*, 17949−17963.

(85) Geiger, R. A.; Leto, D. F.; Chattopadhyay, S.; Dorlet, P.; Anxolabéhère-Mallart, E.; Jackson, T. A. Geometric and Electronic Structures of Peroxomanganese(III) Complexes Supported by Pentadentate Amino-Pyridine and -Imidazole Ligands. *Inorg. Chem.* **2011**, *50*, 10190−10203.

(86) Neese, F. Theoretical spectroscopy of model-nonheme [Fe(IV)OL$_5$]$^{2+}$ complexes in their lowest triplet and quintet states using multireference ab initio and density functional theory methods. *J. Inorg. Biochem.* **2006**, *100*, 716−726.

(87) Liakos, D. G.; Ganyushin, D.; Neese, F. A Multiconfigurational ab Initio Study of the Zero-Field Splitting in the Di- and Trivalent Hexaquo-Chromium Complexes. *Inorg. Chem.* **2009**, *48*, 10572−10580.

(88) Jackson, T. A.; Krzystek, J.; Ozarowski, A.; Wijeratne, G. B.; Wicker, B. F.; Mindiola, D. J.; Telser, J. Vanadocene *de Novo*: Spectroscopic and Computational Analysis of Bis(η5-cyclopentadienyl)vanadium(II). *Organometallics* **2012**, *31*, 8265−8274.

(89) Altun, A.; Breidung, J.; Neese, F.; Thiel, W. Correlated Ab Initio and Density Functional Studies on H$_2$ Activation by FeO$^+$. *J. Chem. Theory Comput.* **2014**, *10*, 3807−3820.

(90) Liptak, M. D.; Fleischhacker, A. S.; Matthews, R. G.; Telser, J.; Brunold, T. C. Spectroscopic and Computational Characterization of the Base-off Forms of Cob(II)alamin. *J. Phys. Chem. B* **2009**, *113*, 5245−5254.

(91) Neese, F.; Petrenko, T.; Ganyushin, D.; Olbrich, G. Advanced aspects of ab initio theoretical optical spectroscopy of transition metal complexes: Multiplets, spin-orbit coupling and resonance Raman intensities. *Coord. Chem. Rev.* **2007**, *251*, 288−327.

(92) Geiger, R. A.; Chattopadhyay, S.; Day, V. W.; Jackson, T. A. A Series of Peroxomanganese(III) Complexes Supported by Tetradentate Aminopyridyl Ligands: Detailed Spectroscopic and Computational Studies. *J. Am. Chem. Soc.* **2010**, *132*, 2821−2831.

(93) Jackson, T. A.; Rohde, J.-U.; Seo, M. S.; Sastri, C. V.; DeHont, R.; Ohta, T.; Stubna, A.; Kitagawa, T.; Münck, E.; Nam, W.; Que, L., Jr. Axial Ligand Effects on the Geometric and Electronic Structures of Nonheme Oxoiron(IV) Complexes. *J. Am. Chem. Soc.* **2008**, *130*, 12394−12407.

(94) Ye, S.; Neese, F.; Ozarowski, A.; Smirnov, D.; Krzystek, J.; Telser, J.; Liao, J.-H.; Hung, C.-H.; Chu, W.-C.; Tsai, Y.-F.; Wang, R.-C.; Chen, K.-Y.; Hsu, H.-F. Family of V(III)-Tristhiolato Complexes Relevant to Functional Models of Vanadium Nitrogenase: Synthesis and Electronic Structure Investigations by Means of High-Frequency and -Field Electron Paramagnetic Resonance Coupled to Quantum Chemical Computations. *Inorg. Chem.* **2010**, *49*, 977−988.

(95) Prins, R.; Van Voorst, J. D. W. Bonding in Sandwich Compounds. *J. Chem. Phys.* **1968**, *49*, 4665−4673.

(96) Ganyushin, D.; Gilka, N.; Taylor, P. R.; Marian, C. M.; Neese, F. The resolution of the identity approximation for calculations of spin-spin contribution to zero-field splitting parameters. *J. Chem. Phys.* **2010**, *132*, 144111.